

Self-Consistent Strong-Coupling-Perturbation Theory for The Anderson Model, Based on Wick's Theorem

Jan Brinckmann

*Institut für Festkörperphysik, Technische Hochschule Darmstadt,
Hochschulstr. 6, D-64289 Darmstadt, Germany*

(Submitted May 24, 1996)

A strong-coupling-perturbation theory around the Atomic Limit of the Anderson model with large U for a localized f -orbital coupled to a conduction-electron band is presented. Although an auxiliary-particle representation is *not* used, application of the canonical Wick's theorem is possible and yields an expansion in the hybridization V via dressed skeleton-Feynman diagrams. The Self-Consistent T-Approximation is constructed as a Φ -derivable approximation. From a numerical solution of self-consistency equations the f -electron-excitation spectrum is investigated. Comparison to the Non-Crossing Approximation is made in virtue of exact formal relations and numerical results. An extension of this Feynman-diagram approach to the Anderson-lattice model is indicated, and application within the Local-Approximation scheme (limit of infinite spatial dimension) is given.

I. INTRODUCTION

Theories of highly correlated electron systems like Kondo Alloys^{1,2}, Heavy-Fermion Systems^{3,4} and High- T_c Superconductors⁵ mostly start from model Hamiltonians like the Anderson or Hubbard model and its extensions⁶⁻⁹. Recently a lot of interest has also been taken in the multi-channel version of the Kondo model¹⁰, to explain non-Fermi-liquid behavior observed in non-magnetic 2-level-impurity systems¹¹⁻¹³ and certain U -based Heavy-Fermion compounds^{14,15}. Common to these models is a single impurity or a lattice of impurities endowed with a local interaction. In Hubbard-like models considered here, electrons on localized d - or f -orbitals experience a Coulomb repulsion U . For the materials mentioned above U is the largest electronic energy, and conventional weak-coupling theories appear not feasible. Besides several mainly numerical techniques, strong-coupling-perturbation theory around the limit of isolated localized orbitals (Atomic Limit) is appropriate for the problem with very large U . The merits of a self-consistent perturbational approach are continuous excitation spectra calculated from Green's functions at the real frequency axis, and the possibility to separate quasi-particle formation from residual interactions. On the other hand, (diagram) rules are required which allow for a partial re-summation of the perturbation series to infinite order. In general this is diffi-

cult to achieve in a strong-coupling approach, where the Coulomb-interaction operator $\sim U$ is part of the unperturbed Hamiltonian, whereas the small hybridization between localized orbitals is taken as the perturbation.

The earliest strong-coupling-perturbation approach¹⁶ deals with time-ordered Goldstone diagrams obtained from an expansion of the Hamiltonian's resolvent¹⁷ without Wick's theorem and is well established for the Anderson-impurity model (for a Review see e.g. Refs. 18,19,2). There is nevertheless enduring interest in alternative approaches, since an extension to e.g. the Anderson-lattice model imposes difficulties on the partial re-summation²⁰⁻²², owing to the use of Goldstone diagrams, i.e. the loss of Wick's theorem. In Slave-Boson theories auxiliary (i.e. unphysical) particles are introduced together with a fluctuating field, which represents the constraint²³. Conventional many-body technique based on Wick's theorem can then be used in the calculation of fluctuation corrections to a saddle point, for impurity and also for lattice models²⁴⁻³⁰. However, one has to start from the Mean-Field ground state (reviewed in e.g. Refs. 31,32), which exhibits broken gauge symmetry³³ with an admixture of unphysical states which influence sum rules^{34,35}. A variety of alternative diagrammatic approaches have been proposed, which start directly from the Atomic Limit rather than the Slave-Boson Mean-Field ground state, like cumulant expansions³⁶⁻⁴⁰, diagram-techniques for Hubbard operators⁴¹⁻⁴⁵, and slave-particle methods where the Mean-Field phase is suppressed in keeping the constraint exact in each order perturbation theory^{46,47}. Other attempts seek Wick's theorem in the limit of zero temperature^{48,49}.

The purpose of this paper is to present a self-consistent skeleton-diagram expansion around the Atomic Limit of the Anderson-impurity model with large U , which is built on Wick's theorem in its conventional form⁵⁰. Neither auxiliary degrees of freedom nor additional constraints are introduced. The theory of lattice models is also considered in the light of this new approach.

In Sect. II an expansion^{51,52} in the hybridization V using conventional Feynman diagrams is re-derived and generalized. The Self-Consistent T-Approximation (SCTA) is constructed in Sect. III as a Conserving Approximation for a set of fermionic Green's functions, and is specialized to the Kondo regime in Sect. IV. Numerical results for the f -excitation spectrum are presented in Sect. V. Here also the relation to the Non-Crossing

Approximation is enlightened via numerical calculations, exact sum rules and spectral decompositions, and a certain limit of the self-consistency (SCTA-) Equations. In Sect. VI we turn to the Anderson-lattice model and investigate the Feynman-diagram expansion on the lattice as well as the application of the so-called Local Approximation. Results are summarized, and conclusions are drawn in Sect. VII. Appendices A to D contain calculational details not included in the main text.

II. EFFECTIVE HAMILTONIAN AND APPLICATION OF WICK'S THEOREM

A. Transformation of The Model Hamiltonian

We start from the Anderson Hamiltonian⁶

$$H = H^c + H^{loc} + H_{01}^V + H_{12}^V$$

of metallic conduction electrons H^c coupled to a localized d - or f -shell H^{loc} through a hybridization term $H_{01}^V + H_{12}^V$:

$$H^c = \sum_{k,\sigma} \varepsilon_{k\sigma} c_{k\sigma}^\dagger c_{k\sigma}, \quad (2.1a)$$

$$H^{loc} = \sum_{\sigma} \varepsilon_{\sigma}^f n_{\sigma}^f + \frac{U}{2} \sum_{\sigma} n_{\sigma}^f n_{-\sigma}^f, \quad (2.1b)$$

$$H_{01}^V = \frac{1}{\sqrt{N_{BZ}}} \sum_{k,\sigma} (1 - n_{-\sigma}^f) (V_k f_{\sigma}^\dagger c_{k\sigma} + h.c.), \quad (2.1c)$$

$$H_{12}^V = \frac{1}{\sqrt{N_{BZ}}} \sum_{k,\sigma} (n_{-\sigma}^f) (V_k f_{\sigma}^\dagger c_{k\sigma} + h.c.). \quad (2.1d)$$

$n_{\sigma}^f = f_{\sigma}^\dagger f_{\sigma}$, and N_{BZ} denotes the number of wave vectors k in the 1. Brillouin zone. The one-particle level ε_{σ}^f of the localized orbital (designated as f -level and f -orbital, respectively) and conduction-electron band-structure $\varepsilon_{k\sigma}$ for spin σ are measured relative to a fixed chemical potential. Conduction electrons form a symmetric band $-D < \varepsilon_k < D$ with cut off D , and the f -level is situated within the filled Fermi sea of conduction electrons, $-D < \varepsilon_{\sigma}^f < 0$. Indices k or σ will be omitted in the following, if appropriate.

The decomposition of the hybridization into H_{01}^V and H_{12}^V is a suitable starting point for strong coupling perturbation theory, where the Atomic ($V_k = 0$) Limit $H^c + H^{loc}$ is taken as the unperturbed Hamiltonian: The first part H_{01}^V of the perturbation induces transitions only within the Fock space sector $\mathcal{H}_{0,1}$ which consists of all states with empty or singly occupied f -orbital. The second part H_{12}^V mixes $\mathcal{H}_{0,1}$ and its complement \mathcal{H}_2 containing all states with double f -occupancy. The sector \mathcal{H}_2 involves the Coulomb repulsion U , and according to the hierarchy

$$V \ll (|\varepsilon^f|, D) \ll U \quad (2.2)$$

it is convenient to eliminate at first H_{12}^V in leading order V/U through a sequence of two canonical transformations. The calculation is outlined in Appendix A and leads to the Hamiltonian

$$H \rightarrow H'' = H^c + H^{loc} + H_{01}^V + H^J. \quad (2.3)$$

In the effective interaction H^J appearing here, an exchange integral is simplified for large U and $V_k = V$ to $J_U := -|V|^2/(\varepsilon^f + U) < 0$,

$$H^J = \frac{1}{N_{BZ}} \sum_{k,q,\sigma} J_U \left(f_{\sigma}^\dagger c_{q,-\sigma}^\dagger f_{-\sigma} c_{k\sigma} + f_{\sigma}^\dagger c_{q,-\sigma}^\dagger c_{k,-\sigma} f_{\sigma} \right) \quad (2.4)$$

The spin part of H^J may also be written as $-2J_U \mathbf{s}^c \cdot \mathbf{s}^f$ and reveals the anti-ferromagnetic coupling of conduction-electron-spin density \mathbf{s}^c to the f -orbital spin \mathbf{s}^f due to virtual excitations into states with doubly occupied f -orbital.

In continuing the sequence of canonical transformations we could also eliminate H_{01}^V and would reproduce the well known Kondo exchange Hamiltonian involving only spin degrees of freedom with a total coupling constant $J^{tot} = |V|^2/\varepsilon^f + J_U$, equivalent to the result of Ref. 53. We do not pursue this way, which is appropriate if the f -level lies well below the conduction band.

An essential result from the above considerations is the fact that the effective Hamiltonian Eq.(2.3) leaves Hilbert space sectors $\mathcal{H}_{0,1}$ and \mathcal{H}_2 decoupled; this enables the expansion in conventional Feynman diagrams given below.

B. Wick's Theorem in Strong-Coupling Expansion

For a study of the Anderson model's one-particle-excitation spectra and transport properties the quantity of interest is the f -Green's function

$$F_{\sigma}(\tau - \tau') = -\langle \mathcal{T} \{ f_{\sigma}(\tau) f_{\sigma}^\dagger(\tau') \} \rangle. \quad (2.5)$$

The symbol $\mathcal{T}\{\dots\}$ orders canonical f -operators $f_{\sigma}^{(\dagger)}$ according to imaginary time τ, τ' ; thermal expectation values $\langle \dots \rangle$ and Heisenberg operators are formed with the Hamiltonian H'' .

By insertion of $1 = (1 - P_2) + P_2$, $P_2 = n_{\uparrow}^f n_{\downarrow}^f$ into Eq.(2.5), the propagator is split into

$$F_{\sigma}(\tau - \tau') = F_{\sigma}^{\text{low}}(\tau - \tau') + F_{\sigma}^{\text{high}}(\tau - \tau'), \quad (2.6)$$

with a low-energy part F^{low} and a high-energy part F^{high} ,

$$F_{\sigma}^{\text{low}}(\tau - \tau') = \quad (2.7)$$

$$-\langle \mathcal{T} \{ ([1 - n_{-\sigma}^f] f_{\sigma})(\tau) ([1 - n_{-\sigma}^f] f_{\sigma}^\dagger)(\tau') \} \rangle,$$

$$F_{\sigma}^{\text{high}}(\tau - \tau') = \quad (2.8)$$

$$-\langle \mathcal{T} \{ (n_{-\sigma}^f f_{\sigma})(\tau) (n_{-\sigma}^f f_{\sigma}^\dagger)(\tau') \} \rangle.$$

The projector P_2 onto subspace \mathcal{H}_2 commutes with H'' ,

$$[P_2, H''] = 0, \quad (2.9)$$

i.e. double f -occupancy is conserved, and therefore mixed terms not written in Eq.(2.6) vanish.

The low-energy part Eq.(2.7) contributes to the one-particle-excitation spectrum $\rho^f(\omega)$ of f -electrons in the frequency range $0 \leq |\omega| < D$ we are interested in, whereas the spectrum of F^{high} is well separated from that by U , due to excitations into \mathcal{H}_2 . Thus the high-energy part will be ignored in the following and we take $F = F^{\text{low}}$, that is

$$F_\sigma(\tau - \tau') = -\frac{1}{Z} \text{Tr}[e^{-\beta H''} \mathcal{T}\{ (f_{-\sigma} f_{-\sigma}^\dagger f_\sigma)(\tau) (f_{-\sigma} f_{-\sigma}^\dagger f_\sigma^\dagger)(\tau') \}] \quad (2.10)$$

with the partition function $Z = \text{Tr}[e^{-\beta H''}]$ and the inverse temperature $\beta = 1/k_B T$.

Our goal is a perturbation expansion of the f -Green's function in the hybridization H_{01}^V and the exchange coupling term H^J appearing in Eq.(2.3). In order to apply Wick's theorem on the course, two points have to be noted: First, on account of the conservation law Eq.(2.9) the Fock-space sector \mathcal{H}_2 involving double f -occupancy is completely decoupled from the dynamics introduced by the perturbation. Second, states from \mathcal{H}_2 do not contribute at all to the trace in Eq.(2.10), owing to Eq.(2.9) and $P_2(f_{-\sigma} f_{-\sigma}^\dagger f_\sigma^\dagger) = (f_{-\sigma} f_{-\sigma}^\dagger f_\sigma^\dagger) P_2 = 0$. Thus the interaction term in the local f -Hamiltonian H^{loc} is completely ineffective, and we may assign any value to the parameter U in H^{loc} , or ignore this interaction term for convenience: $H^{\text{loc}} \rightarrow \tilde{H}^{\text{loc}} = \sum_\sigma \varepsilon_\sigma^f n_\sigma^f$. Accordingly we may work with a modified Hamiltonian $H'' \rightarrow \tilde{H}$,

$$\tilde{H} = \tilde{H}^{(0)} + H_{01}^V + H^J \quad (2.11)$$

where the unperturbed part $\tilde{H}^{(0)}$ is now bilinear in band- and f -operators,

$$\tilde{H}^{(0)} = \sum_{k,\sigma} \varepsilon_{k\sigma} c_{k\sigma}^\dagger c_{k\sigma} + \sum_\sigma \varepsilon_\sigma^f f_\sigma^\dagger f_\sigma. \quad (2.12)$$

Introducing properly normalized expectation values

$$\langle \dots \tilde{\cdot} \rangle \equiv \frac{1}{Z} \text{Tr}[e^{-\beta \tilde{H}} \dots], \quad \tilde{Z} = \text{Tr}[e^{-\beta \tilde{H}}], \quad (2.13)$$

the one-particle Green's function Eq.(2.10) now reads

$$F_\sigma(\tau - \tau') = \frac{\tilde{Z}}{Z} \tilde{F}_\sigma(\tau - \tau'), \quad (2.14)$$

with

$$\tilde{F}_\sigma(\tau - \tau') = -\langle \mathcal{T}\{ (f_{-\sigma} f_{-\sigma}^\dagger f_\sigma)(\tau) (f_{-\sigma} f_{-\sigma}^\dagger f_\sigma^\dagger)(\tau') \} \tilde{\cdot} \rangle. \quad (2.15)$$

In \tilde{F} the thermal average as well as time dependencies of (composite) operators $A(\tau) = e^{\tau \tilde{H}} A e^{-\tau \tilde{H}}$ are determined by the modified Hamiltonian \tilde{H} . Note that double f -occupancy does contribute to \tilde{Z} and therefore \tilde{Z} differs from the partition function Z .

An expansion in connected Feynman diagrams by application of Wick's theorem and linked-cluster theorem is now apparent, since \tilde{F} is a 3-particle Green's function of a fermion system, with an unperturbed Hamiltonian $\tilde{H}^{(0)}$ and a two-particle interaction $H_{01}^V + H^J$ given through Eqs.(2.1c) and (2.4). Following e.g. Ref. 54 a diagram of given order in V and J_U is constructed from bare fermionic Green's functions and the vertices shown in Fig. 1: A dashed line represents a local fermionic Green's function

$$\tilde{G}_\sigma^{f(0)}(i\omega_l) = \frac{1}{i\omega_l - \varepsilon_\sigma^f}, \quad (2.16)$$

with Matsubara frequency $\omega_l = (2l + 1)\pi/\beta$. A full line corresponds to a band electron at the impurity site, with the k -dependence of V_k included,

$$G_\sigma^c(i\omega_l) = \frac{1}{N_{BZ}} \sum_k \frac{|V_k|^2}{V^2} \frac{1}{i\omega_l - \varepsilon_{k\sigma}}. \quad (2.17)$$

For counting the order in perturbation theory a real average V has been introduced,

$$V^2 := \frac{1}{N_{BZ}} \sum_k |V_k|^2. \quad (2.18)$$

Vertices originating from the correlated hybridization H_{01}^V are shown in Fig. 1 (a) and contribute a factor V each, those corresponding to H^J carry a factor J_U , and are depicted in Fig. 1 (b). All vertices conserve direction of arrows (i.e. particle number), spin σ and Matsubara frequency ω_l . Each internal free frequency to be summed up is accompanied by a $1/\beta = k_B T$ and an unusual convergence factor $\exp(-i\omega_l 0_+)$: its exponent differs in sign from standard rules, owing to non-normal ordering of f -operators⁵⁵ in Eq.(2.1c). Sums over internal wave vectors k are always independent and already included in the local band-electron line G^c . The sign $(-1)^{n_c + \chi_{ext} + n_J}$ of a diagram is determined as usual by the number n_c of closed fermion loops, the ordering χ_{ext} of external time labels, and the number n_J of vertices $\sim J_U$. The sign contribution from vertices $\sim V$ is compensated by the non-normal ordering $(1 - n^f) = f f^\dagger$ of f -operators in Eq.(2.1c).

An interpretation of vertices and diagrams in physical processes as indicated in Fig. 1 is obvious, but has to be considered merely as illustrative: The dashed line $\tilde{G}^{f(0)}$ does *not* represent a true bare f -particle $F^{(0)}$ in the unperturbed limit $V = 0$, which is given by⁷

$$F_\sigma^{(0)}(i\omega_l) = \langle 1 - n_{-\sigma}^f \rangle^{(0)} \tilde{G}_\sigma^{f(0)}(i\omega_l);$$

hence the propagator $\tilde{G}^{f(0)}$ lacks the reduced spectral weight factor of $F^{(0)}$. Although this is only a minor effect here, differences become much more pronounced if full propagators are considered.

For the remainder of this paper we turn to the $U \rightarrow \infty$ limit, that is, vertices $\sim J_U$ in Fig. 1 (b) will be dropped according to the Hamiltonian $\tilde{H} \Rightarrow \tilde{H}^{(0)} + H_{01}^V$. The partition function Z is now given through

$$U \rightarrow \infty : \quad Z = \text{Tr}[e^{-\beta H''}] \rightarrow \text{Tr}[e^{-\beta \tilde{H}}(1 - P_2)] \\ = \tilde{Z} - Z^c \exp(-\beta \sum_{\sigma} \varepsilon_{\sigma}^f). \quad (2.19)$$

Thus Z is accessible via an expansion of $\ln(\tilde{Z})$ in linked diagrams. Z^c denotes the partition function of bare conduction electrons.

The Hamiltonian Eq.(2.11) in the limit $U \rightarrow \infty$, i.e. $J = 0$ is well known⁵⁶. It has widely been studied using expansions in the hybridization H_{01}^V via time ordered (Goldstone) diagrams based on the Resolvent Method^{56,23}, or equivalent schemes involving constraints on auxiliary particles^{46,47}. Nevertheless the possibility to apply the canonical Wick's theorem in a strong-coupling expansion has not been realized so far.

Furthermore it is interesting to note that the approach proposed here is easily transferred to the spin-1/2 Kondo model⁵⁷ and multi-channel Kondo model¹⁰, giving rise to a Feynman-diagram representation of the conduction electron's T -matrix: The additional states introduced in writing the local spin in fermions do not contribute to the T -matrix; thus any 'slave-fermion' constraint is unnecessary for a spin-1/2 impurity model, as has already been argued in Ref. 58.

III. SELF-CONSISTENT APPROXIMATION: GENERAL ASPECTS

In the diagrammatic expansion of the 3-particle propagator \tilde{F} , which covers the dynamics of one-particle f -excitations via Eqs.(2.14) and (2.15), we encounter the logarithmic divergences substantial for formation of the Kondo effect⁵⁸. This can already be confirmed for the simplest ladder diagrams shown in Fig. 2, which contribute to \tilde{F} . Details concerning representations of \tilde{F} will be given later on. Consider e.g. the particle-particle (pp) diagram $\gamma^{pp}(i\nu_k)$: Its analytic contribution at bosonic frequency $i\nu_k = 2k\pi/\beta$ is

$$\gamma^{pp}(i\nu_k) \approx V^2 \rho^c(0) \int_{-D}^D d\varepsilon \frac{f(\varepsilon)}{i\nu_k - \varepsilon - \varepsilon^f},$$

where $k_B T \ll |\varepsilon^f|$ and $f(\varepsilon + i\nu_k) = f(\varepsilon)$ denotes the Fermi function. Spin degeneracy has been assumed, and a flat conduction-band density $\rho^c(\varepsilon) = -\frac{1}{\pi} \text{Im} G^c(\varepsilon + i0_+) = \frac{1}{2D} \Theta(D - |\varepsilon|)$ inserted. After continuation to the

real axis, $i\nu_k \rightarrow \omega \pm i0_+$, the real part $\text{Re} \gamma^{pp}(\omega \pm i0_+)$ develops for $T \rightarrow 0$ a logarithmic singularity at the f -level $\omega = \varepsilon^f$. Similar results are obtained for the particle-hole (ph, \overline{ph}) diagrams in Fig. 2.

The strategy to be pursued is quite common to known perturbational strong-coupling approaches²³. Diagrams showing logarithmic divergences have to be resummed, whereby a small Kondo-energy scale in the form $T_A = D \exp(\varepsilon^f/2V^2 \rho^c(0))$ is established^{59,60}. Furthermore a renormalization of propagators in skeleton diagrams is necessary^{61-63,46}, which leads to a smooth Abrikosov-Suhl resonance near the Fermi edge in the f -excitation spectrum and turns T_A towards the exact Kondo energy⁶⁴⁻⁶⁶ T_K . Accordingly we aim at an approximation for the propagator \tilde{F} via summation of a certain class of dressed skeleton-Feynman diagrams⁶⁷ to infinite order in V , involving the diagram elements shown in Fig. 2.

A. Skeleton-Diagram Expansion

To begin with, consider the construction of proper self energies. Since the vertices from Fig. 1 (a) present in the $U \rightarrow \infty$ problem allow for connected diagrams with external lines of arbitrary type, i.e. G^c (c -line, given in Eq.(2.17)) or $\tilde{G}^{f(0)}$ (f -line, see Eq.(2.16)), we get four self energies designated as

$$\Sigma_{\sigma}^{ff}(i\omega_l), \Sigma_{\sigma}^{fc}(i\omega_l), \Sigma_{\sigma}^{cf}(i\omega_l), \Sigma_{\sigma}^{cc}(i\omega_l). \quad (3.1)$$

The type of outgoing and incoming line is indicated in the superscript. As usual, external lines are removed and irreducible (proper) self-energy diagrams cannot be split by cutting only one line of *any* type. Therefore not only a renormalization $\tilde{G}^{f(0)} \rightarrow \tilde{G}^f$ and $G^c \rightarrow \tilde{G}^c$ takes place, but also mixed Green's functions \tilde{G}^{fc} and \tilde{G}^{cf} emerge. The $\tilde{G}^{aa'}$ are depicted as the various kinds of double lines shown in Fig. 3 (a). In the imaginary-time domain, these propagators are defined as

$$\tilde{G}_{\sigma}^f(\tau - \tau') = -\langle \mathcal{T} \{ f_{\sigma}(\tau) f_{\sigma}^{\dagger}(\tau') \} \rangle, \quad (3.2a)$$

$$\tilde{G}_{\sigma}^{fc}(\tau - \tau') = -\langle \mathcal{T} \{ f_{\sigma}(\tau) C_{\sigma}^{\dagger}(\tau') \} \rangle, \quad (3.2b)$$

$$\tilde{G}_{\sigma}^{cf}(\tau - \tau') = -\langle \mathcal{T} \{ C_{\sigma}(\tau) f_{\sigma}^{\dagger}(\tau') \} \rangle, \quad (3.2c)$$

$$\tilde{G}_{\sigma}^c(\tau - \tau') = -\langle \mathcal{T} \{ C_{\sigma}(\tau) C_{\sigma}^{\dagger}(\tau') \} \rangle, \quad (3.2d)$$

with local operators $f_{\sigma}^{(\dagger)}$ and $C_{\sigma}^{(\dagger)} = \frac{1}{\sqrt{N_{BZ}}} \sum_k \frac{V_k^{(*)}}{V} c_{k\sigma}^{(\dagger)}$. Green's functions Eq.(3.2) and corresponding self energies Eq.(3.1) are now collected in a matrix propagator

$$\mathbf{G}_{\sigma}(i\omega_l) = \begin{pmatrix} \tilde{G}_{\sigma}^f & \tilde{G}_{\sigma}^{fc} \\ \tilde{G}_{\sigma}^{cf} & \tilde{G}_{\sigma}^c \end{pmatrix} (i\omega_l) \quad (3.3)$$

and matrix-self energy

$$\Sigma_{\sigma}(i\omega_l) = \begin{pmatrix} \Sigma_{\sigma}^{ff} & \Sigma_{\sigma}^{fc} \\ \Sigma_{\sigma}^{cf} & \Sigma_{\sigma}^{cc} \end{pmatrix} (i\omega_l). \quad (3.4)$$

The bare ($V = 0$) matrix $\mathbf{G}^{(0)}$ contains only diagonal elements $\tilde{G}^{f(0)}$ and G^c since mix-Green's functions $\tilde{G}^{fc/cf}$ vanish in the Atomic Limit. Full and bare matrix-Green's functions are shown in Fig. 3 (b), followed by Dyson's equation in Fig. 3 (c). Diagram rules for matrix propagator and vertex function as well as the vertex in matrix formulation follow from re-writing the perturbation H_{01}^V in 'spinors' $\Psi_\sigma = (f_\sigma, C_\sigma)$, $\bar{\Psi}_\sigma = (f_\sigma^\dagger, C_\sigma^\dagger)$. The resulting vertex is displayed in Fig. 4 (a). At last, we combine the vertex' two possible orientations as shown in Fig. 4 (b). The net result is, that diagram rules for unphysical 'free energy' $\ln(\tilde{Z})$ (see Eq.(2.13)), Green's function \mathbf{G} , self energy Σ and all vertex functions are quite analogous to the interacting electron gas⁵⁴, with an unusual factor⁶⁸ $\exp(-i\omega_n 0_+)$ for each internal frequency ω_n .

Dyson's equation shown in Fig. 3 (c) is written

$$(\mathbf{G}_\sigma(i\omega_l))^{-1} = (\mathbf{G}_\sigma^{(0)}(i\omega_l))^{-1} - \Sigma_\sigma(i\omega_l)$$

and is solved by inversion of a 2×2 -matrix. The elements of \mathbf{G}_σ obtained this way are noted for later use,

$$\tilde{G}_\sigma^{ff} = \frac{1}{[\tilde{G}_\sigma^{f(0)}]^{-1} - \tilde{\Sigma}^f} \quad (3.5a)$$

$$\text{with } \tilde{\Sigma}_\sigma^f = \Sigma_\sigma^{ff} + \frac{\Sigma_\sigma^{fc} \Sigma_\sigma^{cf}}{[G_\sigma^c]^{-1} - \Sigma_\sigma^{cc}}$$

$$\tilde{G}_\sigma^{fc} = \tilde{G}_\sigma^{ff} \frac{\Sigma_\sigma^{fc}}{[G_\sigma^c]^{-1} - \Sigma_\sigma^{cc}} = \frac{\Sigma_\sigma^{fc}}{[\tilde{G}_\sigma^{f(0)}]^{-1} - \Sigma_\sigma^{ff}} \tilde{G}_\sigma^{fc} \quad (3.5b)$$

$$\tilde{G}_\sigma^{cf} = \frac{\Sigma_\sigma^{cf}}{[G_\sigma^c]^{-1} - \Sigma_\sigma^{cc}} \tilde{G}_\sigma^{ff} = \tilde{G}_\sigma^{fc} \frac{\Sigma_\sigma^{cf}}{[\tilde{G}_\sigma^{f(0)}]^{-1} - \Sigma_\sigma^{ff}} \quad (3.5c)$$

$$\tilde{G}_\sigma^c = \frac{1}{[G_\sigma^c]^{-1} - \tilde{\Sigma}^c} \quad (3.5d)$$

$$\text{with } \tilde{\Sigma}_\sigma^c = \Sigma_\sigma^{cc} + \frac{\Sigma_\sigma^{cf} \Sigma_\sigma^{fc}}{[\tilde{G}_\sigma^{f(0)}]^{-1} - \Sigma_\sigma^{ff}}$$

The 3-particle propagator \tilde{F}_σ of Eq.(2.15), which is the quantity that furnishes the f -excitation spectrum, is conveniently expressed through the self energies appearing in Dyson's equation Eq.(3.5): In close analogy to the well known T-matrix relation²³ exact equations of motion are utilized to show that

$$\tilde{G}_\sigma^c(i\omega_l) = G_\sigma^c(i\omega_l) + G_\sigma^c(i\omega_l) V^2 \tilde{F}_\sigma(i\omega_l) G_\sigma^c(i\omega_l), \quad (3.6)$$

with bare and renormalized conduction electron Green's function G_σ^c and \tilde{G}_σ^c , as defined in Eqs.(2.17) and (3.2d) respectively. In combination with Eq.(3.5d) we get the exact expression

$$V^2 \tilde{F}_\sigma(i\omega_l) = \frac{\tilde{\Sigma}_\sigma^c(i\omega_l)}{1 - G_\sigma^c(i\omega_l) \tilde{\Sigma}_\sigma^c(i\omega_l)}. \quad (3.7)$$

Alternatively this result is derived from considering the diagram series of \tilde{F}_σ directly. Apparently $V^2 \tilde{F}$ equals

the *improper* self energy of \tilde{G}^c . Since \tilde{F} stands for a 3-particle propagator, it contains diagrams reducible with respect to band lines G^c (i.e. which can be split by cutting a single G^c) compliant to particle conservation, in contrary to any two-particle Green's function.

B. Mean-Field Theory and Infinite Ladder Summation

The formalism developed so far serves as the basis for defining self-consistent approximations: An expansion of the matrix-self energy Σ in skeleton diagrams with matrix-type lines and vertices leads to *consistent* expressions for its elements $\Sigma^{a'a}$, $a'a = ff, cf, fc, cc$. These fully determine the self-consistency problem via Dyson's equation Eq.(3.5) as well as the one-particle f -Green's function via Eqs. (3.7) and (2.14). As a starting point we take the exact representation^{69,70} for Σ given in Fig. 5. To prevent over-counting the lowest order contribution ('Hartree diagram') is written explicitly, whereas all higher orders are absorbed into the irreducible vertex function⁷¹ Γ_P^2 .

At mean-field level only the 'Hartree diagram' in Fig. 5 is taken into account, which leads to a self energy Σ independent of frequency ω_l . The self-consistency equations resulting from Dyson's equation (3.5) can be solved analytically⁷² at $T \rightarrow 0$. They possess, however, only a trivial solution:

$$\begin{aligned} \Sigma_\sigma^{ff}(i\omega_l) &= 2V \langle f_{-\sigma}^\dagger C_{-\sigma} \rangle \rightarrow 0, \\ \Sigma_\sigma^{cf}(i\omega_l) &= \Sigma_\sigma^{fc}(i\omega_l) = V \langle 1 - n_{-\sigma}^f \rangle \rightarrow 0, \\ \Sigma_\sigma^{cc}(i\omega_l) &= 0. \end{aligned}$$

That is, the unperturbed ($V = 0$) Atomic Limit is recovered in mean-field theory. This result fits into the discussion of the Kondo regime given in Sect. IV below: The lowest order diagram (Fig. 5 left) considered here belongs to a whole class of skeleton diagrams which are negligible in the Kondo regime.

In going to higher orders, attention has to be paid to symmetry relations fulfilled by the vertex function Γ_P^2 : In Fig. 5 the self energy Σ has been given in a way that Γ_P^2 enters Σ in the particle-particle (pp) representation $\Gamma_P^2(1', 2'; 1, 2)$, with arbitrary labels attached to incoming (1, 2) and outgoing (1', 2') lines. Correspondingly it can be analyzed in the (pp)-channel, i.e. re-written through the Bethe-Salpeter equation

$$\begin{aligned} \Gamma_P^2(1', 2'; 1, 2) &= \Gamma^{pp}(1', 2'; 1, 2) \\ &+ \Gamma^{pp}(1', 2'; \bar{1}, \bar{2}) G(\bar{1}, \bar{1}') G(\bar{2}, \bar{2}') \Gamma_P^2(\bar{1}', \bar{2}'; 1, 2), \end{aligned} \quad (3.8)$$

involving a kernel Γ^{pp} which is two-particle irreducible only in the (pp)-channel. An integration $\int d\bar{1} d\bar{2} d\bar{1}' d\bar{2}'$ is implicit, where e.g. $\int d\bar{1}$ is shorthand for $\int_0^\beta d\bar{\tau}_1 \sum(\bar{\sigma}_1 = \pm 1) \sum(\bar{a}_1 = f, c)$. However, the self energy could also be written with reversed arrows on the spin

($-\sigma$) loop in Fig. 5, so that Γ_P^2 would be replaced by its particle-hole (ph) representation $\Gamma^2(1', 1; 2, 2')$. Now two alternative Bethe–Salpeter equations are apparent, where Γ^2 is analyzed in the (ph)- or (\overline{ph})-channel with respective kernels Γ^{ph} and $\overline{\Gamma}^{ph}$,

$$\begin{aligned} \Gamma^2(1', 1; 2, 2') &= \Gamma^{ph}(1', 1; 2, 2') \\ &+ \Gamma^{ph}(1', 1; \overline{2}, \overline{2}') G(\overline{2}, \overline{1}') G(\overline{1}, \overline{2}') \Gamma^2(\overline{1}', \overline{1}; 2, 2') , \end{aligned} \quad (3.9a)$$

$$\begin{aligned} \Gamma^2(1', 1; 2, 2') &= \overline{\Gamma}^{ph}(1', 1; 2, 2') \\ &+ \overline{\Gamma}^{ph}(1', \overline{1}; 2, \overline{2}') G(\overline{1}, \overline{1}') G(\overline{2}, \overline{2}') \Gamma^2(\overline{1}', 1; \overline{2}, 2') . \end{aligned} \quad (3.9b)$$

Additionally an interchange of the two incoming lines of Γ_P^2 in Fig. 5 or, if the particle-hole representation has been chosen, of Γ^2 does not alter Σ , in virtue of the corresponding anti-symmetry of Γ_P^2 , Γ^2 . In combination with the strict equality of particle–particle and particle–hole representations this anti-symmetry is expressed through the so-called Crossing Relations⁷⁰

$$\begin{aligned} \Gamma_P^2(1', 2'; 1, 2) &= -\Gamma_P^2(1', 2'; 2, 1) \\ &= \Gamma^2(1', 1; 2, 2') = -\Gamma^2(1', 2; 1, 2') . \end{aligned} \quad (3.10)$$

These should be fulfilled by any approximation.

A ladder-type approximation to $\Gamma_{(P)}^2$ may be obtained from Eqs. (3.8) and (3.9) with the kernels Γ^{pp} , Γ^{ph} , $\overline{\Gamma}^{ph}$ each replaced by the bare vertex shown in Fig. 4 (b). An iteration of the Bethe–Salpeter equations then yields three different ladder approximations for the vertex function, with diagrams from only one of the three inequivalent channels included. Taking solely one of them into account, with reference e.g. to RPA, does certainly not comply to Crossing Relations. It is more suitable to add all three ladder sums and to remove the lowest order contribution (i.e. the bare vertex) twice afterwards, since it has been counted three times. The resulting vertex function $\Gamma_P^2 = \Gamma^2$ fulfills Crossing Relations (3.10) and contains no over-counted diagram. Furthermore it includes all types of loops from Fig. 2 to infinite order. Eventually, insertion into Fig. 5 leads to the skeleton approximation for the self energy Σ displayed in Fig. 6.

The ladder summation obtained is considerably simple, since solely bosonic propagators representing ladder sums have to be treated self-consistently. A more systematic approach based on Parquet equations^{69,70,73} would involve ‘true’ retarded vertex functions. Additionally the approximation is Φ -derivable, i.e. a functional $\tilde{\Phi}$ can be found⁷³ with the property⁷⁴

$$(\Sigma_\sigma(\tau' - \tau))^{a'a} = \frac{\delta \tilde{\Phi}[\mathbf{G}]}{\delta (\mathbf{G}_\sigma(\tau - \tau'))^{aa'}} . \quad (3.11)$$

Thus *all* self energies $\Sigma^{a'a}$, $a'a = ff, cf, fc, cc$ can be obtained by variation of *one* functional $\tilde{\Phi}$. As a consequence the ladder approximation is thermodynamically consistent⁷⁴, i.e. expectation values $\langle \dots \rangle$ with a *tilde* are

safely computed from corresponding Green’s functions. Since the diagrammatic representation of $\tilde{\Phi}$ resembles that of the T-matrix theory of the electron gas⁶⁷ the self energy Fig. 6 will be referred to as the Self-Consistent T-Approximation (SCTA).

IV. SELF-CONSISTENT SCHEME AND EXCITATION SPECTRUM IN THE KONDO REGIME

So far an approximation for the Anderson model in the strongly correlated limit $U \rightarrow \infty$ has been derived, which does not rely on any specific parameter range such as the Kondo or mixed-valence regime. In the following the Kondo regime will be considered further, where the coupled self-consistency equations given through the matrix Σ and Dyson’s equation Eq.(3.5) may be simplified using a non-perturbative small parameter.

A. Small Parameter

The small parameter available in the Kondo regime is given by the c-number Z/\tilde{Z} , which relates physical quantities like the one-particle f -Green’s function F to its counterpart indexed by a *tilde*, as introduced in Eq.(2.14):

$$F_\sigma(\tau - \tau') = \frac{\tilde{Z}}{Z} \tilde{F}_\sigma(\tau - \tau') . \quad (4.1)$$

At $U \rightarrow \infty$ the prefactor is given through Eq.(2.19),

$$\tilde{Z}/Z = 1 + (Z^c/Z) \exp(-2\beta\varepsilon^f) . \quad (4.2)$$

We estimate the order of magnitude of the partition function Z via

$$Z/Z^c = \exp(-\beta(\Omega - \Omega^c)) \approx \exp(-\beta(E_G - E^c)) ,$$

where the free energy Ω has been replaced at low temperature $T \rightarrow 0$ by the ground-state energy E_G . Quantities Z^c, Ω^c, E^c correspond to bare conduction electrons. As is well known, hybridization lowers the Atomic Limit’s ($V = 0$) ground-state energy $E_G^{(0)} = \varepsilon^f + E^c$ only by the small amount of the Kondo energy T_K to $E_G \approx E_G^{(0)} - T_K$. Thus the estimate $Z/Z^c \approx \exp(-\beta(\varepsilon^f - T_K))$ holds, leading to

$$\frac{\tilde{Z}}{Z} = 1 + \frac{1}{\kappa} \approx \frac{1}{\kappa} , \quad \kappa := \exp(\beta(\varepsilon^f + T_K)) . \quad (4.3)$$

This provides a non-perturbative parameter $\kappa \ll 1$, which is exponentially small in the Kondo regime $\varepsilon^f < 0$, $T_K \ll |\varepsilon^f|$, $k_B T \ll |\varepsilon^f|$. From Eq.(4.1) it now follows that \tilde{F} is of very small magnitude $\sim (\kappa)^1$ (or smaller),

with F being an intensive thermal expectation value $\sim (\kappa)^0 = 1$ (or smaller).

In a similar way information is gained on the mix-Green's functions $\tilde{G}^{cf/fc}$: Following the arguments given after Eq.(2.10), the relation

$$\langle \mathcal{T}\{C_\sigma(\tau)f_\sigma^\dagger(\tau')\} \rangle = \frac{\tilde{Z}}{Z} \langle \mathcal{T}\{C_\sigma(\tau)f_\sigma^\dagger(\tau')\} \tilde{\rangle}$$

holds, together with its complex conjugate involving f_σ and C_σ^\dagger defined below Eq.(3.2). Thus the off-diagonal elements of \mathbf{G} in Eq.(3.3) are of order $\sim (\kappa)^1$,

$$\tilde{G}_\sigma^{fc}(\tau - \tau') \sim (\kappa)^1, \quad \tilde{G}_\sigma^{cf}(\tau - \tau') \sim (\kappa)^1. \quad (4.4)$$

It is also useful to consider directly the spectral weight of F_σ , $\langle 1 - n_\sigma^f \rangle = (\tilde{Z}/Z)\langle 1 - n_\sigma^f \tilde{\rangle}$. It follows that

$$\langle 1 - n_\sigma^f \tilde{\rangle} = \int_{-\infty}^{\infty} d\omega \tilde{\rho}_\sigma^f(\omega)[1 - f(\omega)] \sim \kappa, \quad (4.5)$$

with the Fermi function $f(\omega)$ and the spectral function

$$\tilde{\rho}_\sigma^f(\omega) = -\frac{1}{\pi} \text{Im} \tilde{G}_\sigma^f(\omega + i0_+) > 0. \quad (4.6)$$

Since the integrand in Eq.(4.5) is positive, the function

$$\tilde{\rho}_\sigma^f(\omega)[1 - f(\omega)] \sim (\kappa)^1 \quad (4.7)$$

may serve as a small parameter, too. This property can also be derived from the fact that the spectrum $\tilde{\rho}^f$ develops a threshold behavior at energy $E^{Th} \approx \varepsilon^f + T_K$ when the temperature goes to zero: In Appendix D it is shown that $\tilde{\rho}^f(\omega) \sim \Theta(E^{Th} - \omega)$ at $T = 0$. It is expected that $\tilde{\rho}^f(\omega)$ shows a singularity as ω approaches the threshold E^{Th} from below. Nevertheless, at finite temperature the singularity is removed, and the left hand side of Eq.(4.7) shows its maximum at $\omega \approx E^{Th}$ with a value $\tilde{\rho}^f(E^{Th}) \exp(\beta E^{Th}) \approx \kappa \ll 1$.

With the small quantities Eqs.(4.4) and (4.7) at hand, self-energy diagrams of leading order in κ can be separated from those of higher order in κ , which will be neglected in the Kondo regime. For that purpose we return to the explicit notation using the vertices and Green's functions shown in Figs. 1 (a), 3 (a), and dissolve each matrix-type diagram from Fig. 6 into its contributions to $\Sigma^{a'a}$, $a'a = ff, fc, cf, cc$. Whereas mix-Green's functions contribute directly via Eq.(4.4) a factor κ each, Eq.(4.7) is used within a *loop theorem* proven in Appendix B: A *closed path* in a skeleton diagram to $\Sigma^{a'a}$, which runs exclusively on equally directed Green's functions \tilde{G}^f (double dashed lines), is sufficient for a prefactor κ to that diagram. Vertices may be passed in arbitrary fashion from any incoming dashed line to any outgoing dashed line. Accordingly a *closed path* in general involves lines of either spin direction. As an example two diagrams are shown in Fig. 7 (a) on the top and bottom, which possess one and two non-overlapping closed paths respectively. By application of the *loop theorem* these are

of order $\sim (\kappa)^1$ and $\sim (\kappa)^2$. Closed paths are indicated by dotted lines; in the diagram on the top only one of two equivalent paths is marked as an arbitrary choice.

The resulting subset of ladder diagrams to be considered in the Kondo regime is displayed in Fig. 8 for the diagonal elements of Σ , i.e. Σ^{ff} and Σ^{cc} . Σ^{ff} is $\sim (\kappa)^0 = 1$ because no closed path as described above can be found in the diagrams shown in Fig. 8 (top), nor are any mix-Green's functions \tilde{G}^{fc} or \tilde{G}^{cf} present. The diagrams of (*pp*)-type not shown here as well as all (*ph*)- and (\overline{ph})-diagrams to Σ^{ff} are at least $\sim (\kappa)^1$ by application of the *loop theorem*, i.e. vanishing small in the Kondo regime. Fig. 7 (a) displays examples. Also any diagram containing at least one mix-Green's function \tilde{G}^{fc} or \tilde{G}^{cf} is $\sim (\kappa)^1$ or smaller by Eq.(4.4) and can be neglected. Thereby all diagrams of odd order V^{2n+1} are unimportant, as illustrated in Fig. 7 (b). Σ^{cc} on the other hand is in leading order $\sim (\kappa)^1$: Every diagram of the (*pp*)-type ladder sum indicated in Fig. 8 (bottom) shows one *closed path* on equally directed dashed lines. All (*ph*)- or (\overline{ph})-type ladder graphs to Σ^{cc} not shown here contain at least *two* non-overlapping *closed paths*. These contribute at order $\sim (\kappa)^2$ and are omitted, as well as all diagrams containing at least *two* mix-Green's functions $\tilde{G}^{cf/fc}$. Furthermore, it can be seen that all remaining ladder graphs to Σ^{cc} with only *one* mix-Green's function contain in addition at least one *closed path* on dashed lines and thus are also negligible.

The above-mentioned simplification of the self-consistency problem posed through Dyson's equations Eq.(3.5) follows from the fact that Σ^{ff} is ~ 1 in leading order κ , whereas Σ^{cc} and f - c -mixing self energies are small,

$$\Sigma^{ff} \sim 1, \quad \Sigma^{cf} \sim \Sigma^{fc} \sim (\kappa)^1, \quad \Sigma^{cc} \sim (\kappa)^1. \quad (4.8)$$

This is shown in Appendix B to hold in general for the Kondo regime. Eq.(3.5) now reduces to

$$\tilde{G}_\sigma^f = \left(\left[\tilde{G}_\sigma^{f(0)} \right]^{-1} - \Sigma_\sigma^{ff} \right)^{-1} \sim 1 \quad (4.9)$$

and $\tilde{G}_\sigma^c = G_\sigma^c \sim 1$, $\tilde{G}_\sigma^{fc} \sim \tilde{G}_\sigma^{cf} \sim (\kappa)^1$. Therefore \tilde{G}^f is renormalized self-consistently through Σ^{ff} given in Fig. 8, whereas the conduction-electron Green's function G^c remains bare. The magnitude of mix-Green's functions $\tilde{G}^{fc/cf}$ is reproduced consistently. The latter need not be considered in the Kondo regime.

The local f -Green's function follows from Eqs.(4.1) and (3.7), (3.5d) with (4.8) as

$$F_\sigma(i\omega_l) = \frac{\tilde{Z}}{Z} \frac{\Sigma_\sigma^{cc}(i\omega_l)}{V^2}. \quad (4.10)$$

Although $\Sigma^{cc} \sim (\kappa)^1$ is unimportant for the renormalization of unphysical propagators, it determines the physical f -Green's function F , which in combination with the prefactor Eq.(4.3) is of order 1. The property of Σ being

Φ -derivable stated at the end of the last section, together with Eq.(4.10) takes the form

$$\Sigma_{\sigma}^{ff}(i\omega_l) = \frac{\partial \tilde{\Phi}[\tilde{G}^f, G^c]}{\partial \tilde{G}_{\sigma}^f(i\omega_l)}, \quad F_{\sigma}(i\omega_l) = \frac{\tilde{Z}}{Z} \frac{\partial \tilde{\Phi}[\tilde{G}^f, G^c]}{V^2 \partial G_{\sigma}^c(i\omega_l)}.$$

This corresponds to analogous expressions derived within Resolvent-Perturbation Theory⁶².

B. Self-Consistency Equations

In order to derive analytical expression for self energies, two ‘ladder elements’ are defined as shown in Fig. 9: $\tilde{\pi}(i\nu_k)$ can be understood as an effective bosonic propagator with external frequency $\nu_k = 2k\pi/\beta$, which is further renormalized via a ‘self energy’ $\tilde{\sigma}(i\nu_k)$ to

$$\tilde{\Pi}(i\nu_k) = \frac{\tilde{\pi}(i\nu_k)}{1 - \tilde{\pi}(i\nu_k)\tilde{\sigma}(i\nu_k)}. \quad (4.11)$$

Spin degeneracy is assumed here and in the following, although $\tilde{\Pi}$ is spin-independent in general. The formula corresponding to Fig. 8 (top) then reads

$$\Sigma^{ff}(i\omega_l) = \frac{-1}{\beta} \sum_n V^2 G^c(i\omega_n) \tilde{\Pi}(i\omega_n + i\omega_l) \quad (4.12)$$

with external and free fermionic frequencies ω_l and $\omega_n = (2n + 1)\pi/\beta$ respectively. An overall sign results from the single closed fermion loop in every diagram. With the local DOS of conduction electrons (see Eqs.(2.17) and (2.18)),

$$\rho^c(\varepsilon) = \frac{1}{N_{BZ}} \sum_k \frac{|V_k|^2}{V^2} \delta(\varepsilon - \varepsilon_k), \quad (4.13)$$

and a spectral function of the effective propagator $\tilde{\Pi}$,

$$\tilde{\rho}^{\Pi}(\varepsilon) = -\frac{1}{\pi} \text{Im} \tilde{\Pi}(\varepsilon + i0_+), \quad (4.14)$$

the frequency sum in Eq.(4.12) is performed through a contour integration, leading to

$$\Sigma^{ff}(i\omega_l) = V^2 \iint d\varepsilon d\varepsilon' \rho^c(\varepsilon) \tilde{\rho}^{\Pi}(\varepsilon') \frac{[1 - f(\varepsilon)] + [-1 - g(\varepsilon')]}{i\omega_l + \varepsilon - \varepsilon'}. \quad (4.15)$$

A Bose function $g(\varepsilon')$ appears through $f(\varepsilon' - i\omega_l) = -g(\varepsilon')$. In the numerator a $1 - 1 = 0$ has been added, in order to utilize a property similar to Eq.(4.7),

$$\tilde{\rho}^{\Pi}(\varepsilon)[-1 - g(\varepsilon)] \sim (\kappa)^1. \quad (4.16)$$

Thereby the second term in Eq.(4.15) is of order $\sim (\kappa)^1$ and will be neglected in favor of the first term ~ 1 .

The estimate Eq.(4.16) follows from considering the bosonic Green’s function

$$\tilde{\Pi}(\tau - \tau') = \langle \mathcal{T} \{ (f_{\uparrow} f_{\downarrow})(\tau) (f_{\downarrow}^{\dagger} f_{\uparrow}^{\dagger})(\tau') \} \rangle. \quad (4.17)$$

It acquires the form Eq.(4.11) when its diagrammatic is considered in SCTA for the Kondo regime. In a fashion similar to the argument following Eq.(4.4) we relate this propagator to a suitably chosen thermal expectation value, namely

$$\langle (1 - n_{\uparrow}^f)(1 - n_{\downarrow}^f) \rangle = (\tilde{Z}/Z) \tilde{\Pi}((\tau - \tau') = 0_+).$$

With Eq.(4.3) this results in

$$\int d\varepsilon \tilde{\rho}^{\Pi}(\varepsilon)[-1 - g(\varepsilon)] = \tilde{\Pi}(0_+) \sim (\kappa)^1,$$

and Eq.(4.16) follows since the integrand is always positive⁷⁵. In Appendix C this conclusion is drawn directly from Eq.(4.11). Similar to $\tilde{\rho}^f$ the spectrum $\tilde{\rho}^{\Pi}(\omega)$ shows a threshold behavior at $\omega = E^{Th} \approx \varepsilon^f + T_K$, as is shown in Appendix D. At finite temperature this also implies Eq.(4.16), following the arguments below Eq.(4.7).

The self energy Σ^{ff} is given through the first term of Eq.(4.15) which reads after continuation to complex half planes $i\omega_l \rightarrow z$, $\text{Im}(z) \neq 0$,

$$\Sigma^{ff}(z) = V^2 \int d\varepsilon \rho^c(\varepsilon)[1 - f(\varepsilon)] \tilde{\Pi}(z + \varepsilon). \quad (4.18a)$$

This has to be inserted into \tilde{G}^f given through Eqs.(4.9) and (2.16),

$$\tilde{G}^f(z) = [z - \varepsilon^f - \Sigma^{ff}(z)]^{-1}. \quad (4.18b)$$

The right hand side of Eq.(4.18a) requires

$$\tilde{\Pi}(z) = [\tilde{\pi}(z)^{-1} - \tilde{\sigma}(z)]^{-1}, \quad (4.18c)$$

according to the definition Eq.(4.11). $\tilde{\pi}$ and $\tilde{\sigma}$ given in Fig. 9 complete the set of equations,

$$\tilde{\sigma}(z) = N_J V^2 \int d\varepsilon \rho^c(\varepsilon) f(\varepsilon) \tilde{G}^f(z - \varepsilon), \quad (4.18d)$$

with spin-degeneracy $N_J \equiv 2$, and

$$\tilde{\pi}(z) = \int d\varepsilon \tilde{\rho}^f(\varepsilon)[2f(\varepsilon) - 1] \tilde{G}^f(z - \varepsilon). \quad (4.18e)$$

The latter two expressions follow in leading order $\sim (\kappa)^0$ from Eqs.(C4) derived in Appendix C. The self-consistency equations (4.18) represent the Self-Consistent T-Approximation to the spin-degenerate $U \rightarrow \infty$ Anderson model in the Kondo regime. Parameters are the f -level ε^f , hybridization matrix-element V , the conduction band’s density of states $\rho^c(\varepsilon)$, and the temperature via the Fermi function $f(\varepsilon)$. The Green’s function \tilde{G}^f , or its spectrum $\tilde{\rho}^f(\varepsilon)$ is by construction the independent variable to be determined through a (numerical) solution of Eqs.(4.18).

C. Physical f -Spectrum, Sum Rules

For calculating the f -excitation spectrum we now turn to Σ^{cc} : From inspection of Fig. 8 it follows

$$\Sigma^{cc}(i\omega_l) = V^2 \iint d\varepsilon d\varepsilon' \tilde{\rho}^f(\varepsilon) \tilde{\rho}^\Pi(\varepsilon') \frac{[1 - f(\varepsilon)] + [-1 - g(\varepsilon')]}{i\omega_l + \varepsilon - \varepsilon'},$$

quite analogously to Eq.(4.15). Here, with Eqs.(4.7) and (4.16) both terms of the right hand side are $\sim (\kappa)^1$, and the result fulfills the general property Eq.(4.8). With Eq.(4.10) the f -Green's function follows immediately, and the f -excitation spectrum reads

$$\begin{aligned} \rho^f(\omega) &= -\frac{1}{\pi} \text{Im} F(\omega + i0_+) \\ &= \int d\varepsilon \left[\overline{\tilde{\rho}}^f(\varepsilon) \tilde{\rho}^\Pi(\omega + \varepsilon) + \tilde{\rho}^f(\varepsilon) \overline{\tilde{\rho}}^\Pi(\omega + \varepsilon) \right] \end{aligned} \quad (4.19)$$

Projected Spectra have been introduced here, which are $\sim (\kappa)^0$ and positive for all energies,

$$\overline{\tilde{\rho}}^f(\varepsilon) = \frac{\tilde{Z}}{Z} \tilde{\rho}^f(\varepsilon) [1 - f(\varepsilon)], \quad (4.20a)$$

$$\overline{\tilde{\rho}}^\Pi(\varepsilon) = \frac{\tilde{Z}}{Z} \tilde{\rho}^\Pi(\varepsilon) [-1 - g(\varepsilon)]. \quad (4.20b)$$

It is suitable to use an extra set of equations for $\overline{\tilde{\rho}}^f$ and $\overline{\tilde{\rho}}^\Pi$, in analogy to the Defect Equations in NCA-theory²³. These are derived in Appendix C and read

$$\overline{\tilde{\rho}}^f(\omega) = \left| \tilde{G}^f(\omega) \right|^2 V^2 \int d\varepsilon \rho^c(\varepsilon) f(\varepsilon) \overline{\tilde{\rho}}^\Pi(\omega + \varepsilon), \quad (4.21a)$$

$$\overline{\tilde{\rho}}^\Pi(\omega) = \left| \tilde{\Pi}(\omega) \right|^2 N_J V^2 \int d\varepsilon \rho^c(\varepsilon) [1 - f(\varepsilon)] \overline{\tilde{\rho}}^f(\omega - \varepsilon), \quad (4.21b)$$

with fixed spin degeneracy $N_J \equiv 2$.

For the spectra occurring in Eqs.(4.18) and (4.19), (4.21) a set of exact sum rules is proven in Appendix D. Here we quote the results: The integrated spectral weight of $\tilde{\rho}^f$ and $\tilde{\rho}^\Pi$ is given by

$$\int d\varepsilon \tilde{\rho}^f(\varepsilon) = 1, \quad (4.22a)$$

$$\int d\varepsilon \tilde{\rho}^\Pi(\varepsilon) = 1 - 2 \int d\varepsilon \tilde{\rho}^f(\varepsilon) [1 - f(\varepsilon)], \quad (4.22b)$$

with Eq.(4.5) the weight of $\tilde{\rho}^\Pi$ can be set equal to one. Projected Spectra are related via

$$\int d\varepsilon \left[2\overline{\tilde{\rho}}^f(\varepsilon) - \overline{\tilde{\rho}}^\Pi(\varepsilon) \right] = 1, \quad (4.22c)$$

and the physical f -spectrum is normalized according to

$$\int d\varepsilon \rho^f(\varepsilon) = \langle 1 - n_{\uparrow,\downarrow}^f \rangle = \int d\varepsilon \overline{\tilde{\rho}}^f(\varepsilon). \quad (4.22d)$$

Note that the integrated f -electron spectral weight is not equal to unity, since excitations at high energies $\sim U$ are excluded here; compare to Section II B.

In Appendix D the SCTA is tested against sum rules. It turns out that Eqs.(4.22a) and (4.22b) are strictly fulfilled by the self-consistency equations (4.18), whereas the total f -spectral weight comes out slightly too large, $\int d\varepsilon \rho^f(\varepsilon) = 3 \int d\varepsilon \overline{\tilde{\rho}}^f(\varepsilon) - 1$. Nevertheless, the numerical difference to Eq.(4.22d) is small in the deep Kondo regime, where $\langle n_\sigma^f \rangle \lesssim 1/2$.

V. NUMERICAL RESULTS AND RELATION TO THE NCA

This Section is devoted to numerical results and their interpretation. In addition connections of the SCTA with the Non-Crossing Approximation²³ (NCA) are discussed.

The SCTA-Equations (4.18) have been solved numerically at the real axis $z \rightarrow \omega + i0_+$ through iteration of $\tilde{\rho}^f(\omega)$. After convergence, the proper normalization of $\tilde{\rho}^f$ and $\tilde{\rho}^\Pi$ has been checked. Results shown here correspond to a flat conduction-band DOS $\rho^c(\omega) = \Theta(D - |\omega|)/2D$ with cut-off D and parameters $D = 10.0\Delta$, $\varepsilon^f = -3.0\Delta$, $N_J \equiv 2$ in the Kondo regime, where $\Delta = \pi V^2 \rho^c(0)$ denotes the energy scale of the non-interacting impurity model. The Kondo energy^{64,76} takes a value $T_K \approx 0.016\Delta$. In Fig. 10 the spectra $\tilde{\rho}^f$ and $\tilde{\rho}^\Pi$ are displayed for a temperature $k_B T = 0.1T_K$. A threshold behavior, which has been shown above to be a feature of these spectra at $T \rightarrow 0$ (see also Appendix D) shows up in the form of a sharp resonance near the bare f -level ε^f . The Projected Spectra $\overline{\tilde{\rho}}^f$, $\overline{\tilde{\rho}}^\Pi$ are obtained by iteration of Eqs.(4.21) and have been normalized according to Eq.(4.22c) (a common prefactor is arbitrary in Eqs.(4.21)). From Eq.(4.19) then follows the f -excitation spectrum ρ^f . Since it does not strictly fulfill its sum rule Eq.(4.22d), the latter has been used to enforce the correct norm of ρ^f .

In Fig. 11 the calculated f -spectrum is shown, together with an NCA result for the same set of parameters and temperature. It shows the well known features, a 'charge resonance' (CR) near the f -level and a sharp Abrikosov-Suhl resonance (ASR) near the Fermi edge $\omega = 0$. In SCTA the CR is located slightly above $\varepsilon^f = -3.0\Delta$, which is in contradiction to intuition (the gain in kinetic energy due to hybridization should *lower* the f -level) and the NCA result. Obviously, in SCTA some spectral weight is transferred to energies near the Fermi level, and the amplitude of the ASR is in general too high. As a consequence local Fermi-liquid properties⁷⁷ and the Friedel-Langreth sum-rule⁷⁸ are not fulfilled. The f -valence $N_J \langle n_\sigma^f \rangle$ as derived from Eq.(4.22d) takes a value ≈ 0.66 too small for the Kondo regime. As an origin of the misplaced spectral weight in the f -excitation

spectrum ρ^f we might take the representation of the f -Green's function in SCTA, i.e. the self energy Σ^{cc} as displayed in Fig. 8 (bottom), since it violates the normalization rule Eq.(4.22d). On the other hand, the characteristic shape of the 'charge resonance' is already obvious in $\tilde{\rho}^{\text{II}}$ shown in Fig. 10, which results solely from Σ^{ff} (depicted in Fig. 8 top) and enters ρ^f through the convolution in Eq.(4.19). Also the f -valence is computed directly from $\tilde{\rho}^f$ via the sum rule Eq.(4.22d) and does not involve Σ^{cc} either.

Some insight may be gained from a certain non-systematic limit of the SCTA, which reproduces the NCA: If the ladder structure in Σ^{ff} or Σ^{cc} (see Fig. 8) is read from the left to the right, the 'ladder element' $\tilde{\pi}$ (displayed in Fig. 9 left) could be viewed as two holes of opposite spin coexisting in the f -orbital. This empty-orbital state then would be renormalized through intermediate particle-hole excited states with single f -occupancy, represented by $\tilde{\sigma}$ (see Fig. 9 right). Following this interpretation, our bosonic Green's function $\tilde{\Pi}(z)$ appears similar to the NCA-propagator $G_0(z)$ for the empty f -orbital⁷⁹. In fact, if the renormalization of lines within $\tilde{\pi}$ is ignored (NCA Limit),

$$\tilde{\pi}(z) \rightarrow \tilde{\pi}^{\text{NCA}}(z) := 1/[z - 2\varepsilon^f],$$

the NCA equations²³ are reproduced after a re-definition of $z \rightarrow z' = 2\varepsilon^f - z$. Although the interpretation outlined above seems obvious, it may only serve as an instructive starting point, because the Green's function \tilde{G}^f (the dashed double line in diagrams) does *not* represent any physical particle. The 'formal meaning' of both $\tilde{\Pi}$ and \tilde{G}^f has to be viewed quite analogously to unphysical propagators G_0 and G_1 of Resolvent-Perturbation Theory. In the limit of zero temperature this analogy even turns to an equality, as is argued in Appendix D. Nevertheless, in general both approaches are quite different, which is apparent if the definitions of Green's functions and spectra in Eqs.(3.2a), (4.17), (4.20) and sum rules Eqs.(4.22) are compared to their respective counterparts of the Resolvent Method (see e.g. Ref. 79). Most striking are the completely different diagram rules and the explicit use of the Kondo regime within the approach presented here.

Utilizing the NCA Limit the unexpected shape of the 'charge resonance' (CR) in SCTA is traced back to the self energy Σ^{ff} : In the NCA Limit the 'ladder element' $\tilde{\pi}$ shows an imaginary part $-\text{Im} \tilde{\pi}^{\text{NCA}}(\omega + i0_+) = \pi\delta(\omega - 2\varepsilon^f)$ sharply peaked around $2\varepsilon^f$, which leads to the NCA-curve in Fig. 11. In going to the ladder approximation, this is replaced by $-\text{Im} \tilde{\pi}(\omega + i0_+) = \pi \int d\varepsilon \tilde{\rho}^f(\varepsilon) \tilde{\rho}^f(\omega - \varepsilon)$. Accordingly $-\text{Im} \tilde{\pi}$ has a broadened shape like $\tilde{\rho}^f$ displayed in Fig. 10 (full line), with the peak located above $2\varepsilon^f$. Hence the CR in ρ^f is shifted to higher frequencies and gets the asymmetric shape visible in the SCTA-curve in Fig. 11. A few more conclusions are drawn in the Summary.

VI. APPLICATION TO THE LATTICE MODEL

A. Elementary Perturbation Expansion

The strong-coupling-perturbation expansion for the Anderson-lattice model, as the generic model for e.g. Heavy-Fermion Systems is discussed from the Feynman-diagram technique's point of view. The main difficulty encountered when performing an expansion around the Atomic Limit of lattice models is the so-called Excluded-Volume Problem⁸⁰ (EVP), which hinders the application of the Linked-Cluster Theorem: Within the Resolvent-Perturbation formalism all parts of a lattice-diagram which involve a certain f -orbital site $R_i \equiv i$ are necessarily linked together²⁰. Accordingly diagrams have to be broken up ('decoupled') into unlinked diagrams^{81,21} in order to obtain an expansion of thermal densities like the (site dependent) lattice f -Green's function F_{ij}^{lat} through connected diagrams, leading to the known LNCA^{22,82} and XNCA⁸³ schemes. Specifying quasi particle interactions (cumulants) consistently remains a difficult task²². We consider here the lattice model in a fashion analogous to the impurity treatment in Sect. II. It shall turn out, although Feynman-diagrams are obtained, that the EVP cannot be avoided completely; nevertheless it takes a much 'weaker' form than in Resolvent-Perturbation Theory.

After having decoupled states with at least one doubly occupied f -orbital from those with no double f -occupancy via a canonical transformation of the Anderson-lattice Hamiltonian in leading order V/U , we arrive at an expression for $F_{ij,\sigma}^{\text{lat}}$ similar to Eq.(2.10). For large U , i.e. $J = 0$ it reads in the interaction picture

$$\begin{aligned} F_{ij,\sigma}^{\text{lat}}(\tau, \tau') &= - \left(\tilde{Z}^{\text{lat}(0)} / Z^{\text{lat}} \right) \quad (6.1) \\ &\times \left\langle \mathcal{T} \left\{ \exp \left(- \int_0^\beta d\bar{\tau} \sum_i H_{01;i}^V(\bar{\tau}) \right) \right. \right. \\ &\times \left. \left. (f_{i,-\sigma} f_{i,-\sigma}^\dagger)(\tau) (f_{j,-\sigma} f_{j,-\sigma}^\dagger)(\tau') \right\} \right. \\ &\times \left. \prod_{\mu \neq i,j} e^{-\beta U n_{\mu\uparrow}^f n_{\mu\downarrow}^f} \right\rangle^{\tilde{\text{lat}}(0)} \end{aligned}$$

with $\tilde{Z}^{\text{lat}(0)} = \text{Tr}[\exp(-\beta \tilde{H}^{\text{lat}(0)})]$. The unperturbed (atomic) lattice Hamiltonian is split into the bilinear part

$$\tilde{H}^{\text{lat}(0)} = \sum_{k,\sigma} \varepsilon_k c_{k\sigma}^\dagger c_{k\sigma} + \sum_{i,\sigma} \varepsilon_\sigma^f f_{i\sigma}^\dagger f_{i\sigma}$$

and the local f -repulsion $\sim U$. The latter does not influence the time dependent operators occurring in Eq.(6.1) and appears only in the product of e -factors. The perturbations $H_{01;i}^V$ are generalizations of Eq.(2.1c) for each site $i = 1, \dots, N_{BZ}$. Due to the fact that states with double local f -occupancy do contribute to the trace for all lattice sites μ different from i and j , the e -factors in

general cannot be set equal to unity, in contrast to the single site $i = j \equiv 1$ problem. The contribution of order V^n to the perturbation series arising from Eq.(6.1) is proportional to

$$\langle \mathcal{T} \{ H_{01;i_1}^V \dots H_{01;i_n}^V \cdot (\dots i \dots)(\tau) \cdot (\dots j \dots)(\tau') \} \rangle^{\widetilde{lat}(0)} \times \prod_{\mu \notin L} \langle e^{-\beta U n_{\mu\uparrow}^f n_{\mu\downarrow}^f} \rangle^{\widetilde{lat}(0)}, \quad (6.2)$$

where time variables to be integrated out are omitted. Site indices $i_1, \dots, i_n; i, j$ are kept fixed for the moment and are assumed to cover a certain set $L = \{\nu_1, \nu_2, \dots, \nu_l\}$ of $l \leq (n+2)$ *mutual distinct* lattice sites. Accordingly the e -factors from Eq.(6.1) for all sites $\bar{\mu} \in L$ act as unity since double f -occupancy is projected out by $H_{01;\bar{\mu}}^V$, and the expression takes the factorized form Eq.(6.2). Wick's theorem is now applicable to the first term in Eq.(6.2), whereas the second term yields an additional c -number, $\prod_{\mu \notin L} \langle \dots \rangle^{\widetilde{lat}(0)} = (\sum_{\sigma} e^{\beta \varepsilon_{\sigma}^f})^{(n-l)}$ for $k_B T \ll |\varepsilon^f|$. That is, a bookkeeping of the *number l of distinct sites* involved has to take place when sums over site indices are performed. This 'weak form' of the Excluded-Volume Problem prevents the conventional direct cancelation of disconnected Feynman diagrams in the lattice f -Green's function. Nevertheless an expansion in Feynman diagrams is gained, i.e. any kind of 'decoupling' of lattice diagrams becomes unnecessary. Possible applications will be indicated in Sect. VII.

B. Local Approximation

A from the outset more approximative approach to lattice models is the well known Local Approximation (also referred to as Dynamical Mean-Field Theory), which emerges from considerations of the limit of infinite spatial dimension^{84,85} ($d \rightarrow \infty$) via weak-coupling-perturbational and -functional methods (see e.g. Ref. 86–92) as well as strong-coupling-perturbation theories^{37,38,51} doing with Hubbard cumulants³⁶. For the Anderson-lattice model the different $d \rightarrow \infty$ -approaches^{87,93,51} lead to identical results^{51,94}, which becomes obvious if self-energies are eliminated from equations in Refs. 87,93. The lattice f -Green's function $F_{k\sigma}^{lat}$ in k -space turns out equivalent to the XNCA expression⁸³,

$$F_{k\sigma}^{lat}(z) = \left[(F_{\sigma}(z))^{-1} - V^2 \left(\frac{1}{z - \varepsilon_k} - \mathcal{G}_{\sigma}^c(z) \right) \right]^{-1}$$

with an effective impurity (EI) model's conduction-electron Green's function \mathcal{G}_{σ}^c determined through the lattice-self-consistency condition (Lattice-SC), $\frac{1}{N_{BZ}} \sum_k F_{k\sigma}^{lat}(z) = F_{\sigma}(z)$. The EI model f -Green's function is designated as F_{σ} . In calculating F_{σ} numerically via the SCTA theory within a

loop that iterates \mathcal{G}_{σ}^c to convergence, the approach described in previous Sections is extended to the $U \rightarrow \infty$ Anderson-lattice model. Unfortunately we encounter a difficulty well known from the XNCA⁸³: Except at extremely high temperatures the spectrum of \mathcal{G}_{σ}^c develops a peak structure near the Fermi level, indicating an enhancement of the Kondo effect⁹⁵; but if \mathcal{G}_{σ}^c is re-inserted into the SCTA, the spectrum of F_{σ} does not alter significantly, i.e. it does not show any tendency toward a hybridization gap in the Abrikosov–Suhl resonance. Consequently the Lattice-SC cannot be fulfilled. Comments on this result are given in the following Summary.

VII. SUMMARY AND CONCLUSIONS

A detailed description of a self-consistent strong-coupling-perturbation theory for the Anderson model has been given, which extends a Feynman-diagram technique proposed recently^{51,52}. It was shown in Sect. II that Wick's theorem can be applied *directly* within a perturbation expansion in the hybridization V , i.e. the coupling of a localized orbital (f -orbital) to delocalized conduction-electron states. Although the strong Coulomb interaction U of electrons on the f -orbital is included in the unperturbed Atomic Limit, conventional Feynman-diagram rules are obtained in the sequel, involving the two-particle vertices $\sim V$ and $\sim V^2/U$ shown in Fig. 1. This kind of Feynman-perturbation theory starts from a canonical transformation of the Hamiltonian, which eliminates in leading order V/U the charge fluctuations into states with double f -occupancy. It has also been pointed out in Sect. II that an application to the (multi channel) Kondo model is apparent.

Based on the diagram rules for $U \rightarrow \infty$ the Self-Consistent T-Approximation (SCTA) has been derived in Sect. III. By means of irreducible vertex functions compliant to symmetry relations (Crossing Relations) a matrix-type self energy Σ has been set up; it is displayed in Figs. 5, 6. This skeleton-self energy constitutes a Φ -derivable approximation for a set of unphysical propagators as well as a prescription for constructing the physical f -Green's function from these propagators. It contains ladder sums of the diagram elements shown in Fig. 2 to infinite order V ; the latter have been identified as important for the formation of the Kondo effect. A version of the SCTA suitable for the Kondo regime emerged in Sect. IV from an expansion of Σ in a non-perturbative small parameter. Only one of the unphysical Green's functions remains renormalized in this case, represented through the self-consistent SCTA-Equations (4.18). Some relations to the Non-Crossing Approximation (NCA) were explored in Sect. V. Furthermore the SCTA contains the NCA as a certain non-systematic limit.

The numerical results for the physical f -Green's function presented in Sect. V reproduce the known correlation-induced features of the f -excitation spec-

trum. Concerning Fermi-liquid properties, it became apparent that the SCTA does not furnish results which improve those of the NCA. Nevertheless, the formulation of enhanced approximations will be straight forward since standard techniques for Feynman diagrams (e.g. Parquet equations) can be used, and the expansion for the Kondo regime is not restricted to specific diagram classes (see Appendix B). Going beyond the summation of ladder diagrams in the Φ -functional will involve ‘true’ retarded vertex functions. The importance of vertex corrections to the NCA has already been pointed out^{76,96,97}. Here vertex corrections to the matrix-type self energy Σ yield a consistent modification of the self-consistency equations as well as the representation of the physical f -Green’s function. Actually both have significant influence on the f -spectrum and require corrections, as has been argued in Sect. V. Further studies based on the technique developed here might therefore be fruitful with regard to dynamical properties of the spin-degenerate model in the problematic region of very low temperature.

Two possible ways of extending the technique to the ($U \rightarrow \infty$) Anderson-lattice model, an elementary perturbation expansion on the lattice and the application within the Local Approximation, have been discussed in Sects. VIA and VIB respectively. For the elementary expansion it turned out that any contribution to the f -Green’s function is indeed decomposed into Feynman diagrams by virtue of Wick’s theorem, but in addition the number of mutual different f -orbital sites actually involved enters through a c -number (‘weak’ Excluded-Volume Problem). Thus an expansion in connected diagrams may not be obtained in a simple fashion. Nevertheless, the definition of quasi particles and their interactions seems manageable. Accordingly the approach looks quite suitable for models with a small number of impurities with local interaction, e.g. the two-impurity multi-channel Kondo model⁹⁸. Concerning the Anderson-lattice and t - J -model we believe that our method will also show some impact, especially on the study of non-local spin fluctuations via strong-coupling theory for e.g. High- T_c -Superconductors^{99,100} or Heavy-Fermion Systems near a quantum-phase transition^{101,15}.

In the Local Approximation (or Dynamical Mean-Field Theory, reviewed briefly in Sect. VIB) the f -Green’s function of the lattice model is given through that of an effective impurity (EI) model subject to a lattice-self-consistency condition (Lattice-SC). The SCTA equations from Sect. IV were used to solve the EI model, but convergence to the Lattice-SC has not been achieved; a feature already known from the NCA within Local Approximation (i.e. the XNCA)⁹⁴. Such a behavior is not found if the Lattice-SC for the Anderson-lattice model is combined with methods different from strong-coupling perturbation theory (e.g. QMC^{102,103}, numerical diagonalization¹⁰⁴ or weak-coupling perturbation theory^{105,106}), or if strong-coupling theory is used within a different Lattice-SC for the same model, as is the case of the LNCA^{82,94}. In order to clarify this in-

consistent situation we propose considering alternative strong-coupling expansions for the lattice model, which do not rely on the Local Approximation or the Resolvent Method. The elementary expansion outlined in Sect. VIA may serve as a starting point.

ACKNOWLEDGMENTS

The author wishes to thank Prof. N. Grewe for many valuable discussions on the subject of this work and support during preparation of the manuscript. A critical reading of the manuscript by Drs. F. Anders and Th. Pruschke has been greatly appreciated. Useful conversation to Profs. P. Wölfle and J. Keller, and Drs. T. A. Costi and T. Kopp is also gratefully acknowledged.

APPENDIX A: EFFECTIVE HAMILTONIAN

An effective Hamiltonian H'' , where the mixing H_{12}^V involving local double occupation is removed to first order V/U is derived from Eq.(2.1) in two steps: The first unitary transformation^{53,107} is $H \rightarrow H'$,

$$H' = e^{iS} H e^{-iS} = H + [iS, H] + \frac{1}{2}[iS, [iS, H]] + \dots$$

with a generator iS subject to the requirement

$$[iS, (H^c + H^{loc})] = -H_{12}^V.$$

An appropriate choice is

$$iS = \frac{1}{\sqrt{N_{BZ}}} \sum_{k,\sigma} \mathcal{J}_\sigma(k) n_{-\sigma}^f f_{\sigma}^\dagger c_{k\sigma} - h.c. \quad (A1)$$

with $\mathcal{J}_\sigma(k) = V_k / (\varepsilon_\sigma^f + U - \varepsilon_{k\sigma})$. Since H_{01}^V is kept in H' , additional operators mixing Hilbert space sectors $\mathcal{H}_{0,1}$ and \mathcal{H}_2 emerge through $[iS, H_{01}^V]$, which is of order V/U . To this order they vanish in a second transformation

$$H' \rightarrow H'' = H' + [iS', H'] + \dots$$

using a generator iS' which fulfills

$$[iS', (H^c + H^{loc})] = -[iS, H_{01}^V].$$

It is explicitly given by

$$iS' = \frac{1}{N_{BZ}} \sum_{k,q,\sigma} \mathcal{K}_\sigma(k, q) f_{\sigma}^\dagger f_{-\sigma}^\dagger c_{q,-\sigma} c_{k\sigma} - h.c.$$

involving coefficients $\mathcal{K}_\sigma(k, q)$ of order V^2/U^2 . The resulting effective Hamiltonian H'' reads to first order V/U ,

$$H'' = H^c + H^{loc} + H_{01}^V + H^J,$$

where the Coulomb repulsion U in H^{loc} is slightly shifted,

$$U \rightarrow U' = U + \frac{1}{N_{BZ}} \sum_{k,\sigma} \frac{|V_k|^2}{\varepsilon_\sigma^f + U - \varepsilon_{k\sigma}}$$

and a spin-spin interaction emerges, which is part of

$$H^J = \frac{1}{N_{BZ}} \sum_{k,q,\sigma} \frac{1}{2} (-\mathcal{J}_\sigma(k) V_q^*) \cdot \left(f_\sigma^\dagger c_{q,-\sigma}^\dagger f_{-\sigma} c_{k\sigma} + f_\sigma^\dagger c_{q,-\sigma}^\dagger c_{k,-\sigma} f_\sigma \right) + h.c.$$

The exchange integral originating from Eq.(A1) is simplified for large U and $V_k = V$ to

$$\mathcal{J}_\sigma(k) V_q^* \approx |V|^2 / (\varepsilon^f + U) \equiv -J_U,$$

and H^J takes the form Eq.(2.4).

APPENDIX B: THE LOOP THEOREM

In Section IV counting of a certain kind of loops is used to separate out important self-energy diagrams for the Kondo regime. The underlying ‘loop theorem’ for skeleton diagrams is derived as follows. Consider a *closed path* in an arbitrary diagram, as introduced in Section IV below Eq.(4.7): It consists solely of equally directed renormalized Green’s functions \tilde{G}^f (dashed double lines, see Fig. 3) and vertices as displayed in Fig. 1 (a). Vertices may be passed from any incoming dashed line to any outgoing dashed line, i.e. the path may involve both spin directions. None of the diagram’s lines and vertices is to be touched more than once. In Fig. 7 (a) some examples are shown. The analytical contribution from a *closed path* running on k dashed double lines involves also k distinct vertices and is proportional to

$$L^{(k)} = \pm \frac{1}{\beta} \sum_{\omega_n} e^{-i\omega_n 0^+} \left[\tilde{G}^f(i\omega_n - i\nu_1) \dots \tilde{G}^f(i\omega_n - i\nu_k) \right]. \quad (\text{B1})$$

It is coupled to the remainder of the diagram through k fixed bosonic frequencies labeled ν_1, \dots, ν_k . These are kept unequal in pairs through suitably fixed infinitesimal increments¹⁸ $\nu_l \rightarrow \nu_l + \delta_l$. The sum over the free fermionic loop-frequency ω_n is rewritten as usual⁵⁴,

$$L^{(k)} = \mp \int d\varepsilon_1 \dots \varepsilon_k \tilde{\rho}^f(\varepsilon_1) \dots \tilde{\rho}^f(\varepsilon_k) \times \oint_{\Gamma} \frac{dz}{2\pi i} \frac{[1 - f(z)]}{(z - i\nu_1 - \varepsilon_1) \dots (z - i\nu_k - \varepsilon_k)},$$

where \tilde{G}^f is expressed via its spectrum Eq.(4.6). The contour Γ encircles all zeros of the denominator. The term $[1 - f(z)]$ is a consequence of the exponential factor in Eq.(B1), which keeps track of non-normal ordering of operators (ref. Sect. II B). Performing the contour integral leads to

$$L^{(k)} = \mp \sum_{l=1}^k \int d\varepsilon_l \tilde{\rho}^f(\varepsilon_l) [1 - f(\varepsilon_l)] \prod_{l' \neq l} \tilde{G}^f(\varepsilon_l + i\nu_{l'} - i\nu_{l'})$$

Now all other free frequencies in the diagram are integrated out one after the other, and the diagram appears as a sum over k terms. These are regular for finite temperature, and the infinitesimal increments introduced above become unnecessary. The function $\tilde{\rho}^f(\varepsilon)[1 - f(\varepsilon)] \sim \kappa$ discussed in Section IV shows up in each term here and gives the diagram the small overall order of magnitude $\kappa = \exp(\beta(\varepsilon^f + T_K))$ in the Kondo regime. The argument becomes apparently invalid if at least one of the Green’s functions \tilde{G}^f on the path is reversed in orientation, i.e. $\tilde{\rho}^f(\varepsilon) \rightarrow \tilde{\rho}^f(-\varepsilon)$, or is replaced by a conduction-electron propagator $\tilde{\rho}^f(\varepsilon) \rightarrow \rho^c(\varepsilon)$. In a straight-forward generalization, the resulting ‘loop theorem’ is stated: p non-overlapping *closed directed paths* in a skeleton diagram are *sufficient* for an order of magnitude $\sim (\kappa)^p$.

As an application we determine the order of magnitude of self energies $\Sigma^{a'a}$, $a'a = ff, cf, fc, cc$, without reference to any specific approximation. The result has been quoted in Eq.(4.8). Consider at first a diagram to Σ^{cc} , or more generally an arbitrary connected dressed skeleton diagram with one incoming and one outgoing conduction-electron line G^c . It shows necessarily at least one *closed path* as defined above: We construct a path running solely on dashed lines \tilde{G}^f , starting on an outgoing dashed line of an arbitrary chosen vertex within the diagram. We always follow the direction of arrows, and no line or vertex is visited twice. Owing to the fact that a vertex (displayed in Fig. 1 (a) left or right) entered on the way can be left via at least one dashed line, the path cannot terminate within the diagram. Therefore (i) the procedure can lead back to the vertex we started from, and a *closed path* is completed; (ii) a vertex with two incoming dashed lines (Fig. 1 (a) right) is re-entered for the first time on its hitherto unused line, which constitutes a *closed path*, too; (iii) the path we are constructing leaves the diagram via an external outgoing dashed line, if present. Possibility (iii) is ruled out for the diagrams to Σ^{cc} , therefore these contain at least one *closed path* which contributes a factor κ to the self energy’s order of magnitude. Diagrams showing exactly one such path are easily found (see Fig. 8 bottom), and it follows that in general $\Sigma^{cc} \sim (\kappa)^1$. In quite the same way it is seen that $\Sigma^{cf} \sim (\kappa)^1$ and $\Sigma^{fc} \sim (\kappa)^1$. For the latter a *closed path* is constructed starting on an incoming line of an arbitrary chosen internal vertex and proceeding in opposite direction to arrows. The situation is altered if Σ^{ff} is considered: Here a path can leave the diagram (case (iii)), that is Σ^{ff} may contain diagrams of order $\sim (\kappa)^0 = 1$. Actually such diagrams do exist (e.g. those shown in Fig. 8 top), thus $\Sigma^{ff} \sim (\kappa)^0$.

APPENDIX C: EQUATIONS FOR PROJECTED SPECTRA

A set of self-consistency equations is derived for the Projected Spectra introduced in Section IV. According to the definition of $\overline{\rho}^f$ in Eq.(4.20a) we consider

$$\begin{aligned} \tilde{\rho}^f(\omega)[1 - f(\omega)] = \\ \left| \tilde{G}^f(\omega) \right|^2 \left(-\frac{1}{\pi} \right) \text{Im} \Sigma^{ff}(\omega + i0_+) [1 - f(\omega)] , \end{aligned}$$

where Eq.(4.18b) has been used with $z = \omega + i0_+$. The self energy's imaginary part is taken from Eq.(4.15) at $i\omega_l \rightarrow \omega + i0_+$,

$$\begin{aligned} \tilde{\rho}^f(\omega)[1 - f(\omega)] = \left| \tilde{G}^f(\omega) \right|^2 \\ \times V^2 \int d\varepsilon \rho^c(\varepsilon) \tilde{\rho}^\Pi(\varepsilon + \omega) [-f(\varepsilon) - g(\varepsilon + \omega)] f(-\omega) , \end{aligned} \quad (\text{C1})$$

with $1 - f(\omega) = f(-\omega)$. For further transformation of expressions like this, a couple of relations involving Bose and Fermi functions (designated as g and f) is useful,

$$g(x - y) = f(x)[1 - f(y)] / [f(y) - f(x)] , \quad (\text{C2a})$$

$$f(x - y) = f(x)[1 + g(y)] / [g(y) + f(x)] . \quad (\text{C2b})$$

For use in Eq.(C1) the former is applied to $g(\varepsilon + \omega)$ in the first row of the right hand side in

$$\begin{aligned} [\dots] f(-\omega) = [-f(\varepsilon) - g(\varepsilon + \omega)] [f(-\omega) - f(\varepsilon)] \\ + [-f(\varepsilon) - g(\varepsilon + \omega)] f(\varepsilon) \\ = f(\varepsilon) [-1 - g(\varepsilon + \omega)] . \end{aligned}$$

Thereby Eq.(C1) becomes

$$\begin{aligned} \tilde{\rho}^f(\omega)[1 - f(\omega)] = \left| \tilde{G}^f(\omega) \right|^2 \\ \times V^2 \int d\varepsilon \rho^c(\varepsilon) f(\varepsilon) \tilde{\rho}^\Pi(\varepsilon + \omega) [-1 - g(\varepsilon + \omega)] . \end{aligned} \quad (\text{C3})$$

By multiplying \tilde{Z}/Z to both sides Equation (4.21a) is obtained immediately.

Its counterpart Eq.(4.21b) is derived in a similar fashion: With Eq.(4.11) the spectrum $\tilde{\rho}^\Pi(\omega)$ is written

$$\tilde{\rho}^\Pi = -\frac{1}{\pi} \text{Im} \left(\tilde{\Pi} \right) = \left| \tilde{\Pi} \right|^2 \left\{ \frac{-\text{Im}(\tilde{\pi})/\pi}{|\tilde{\pi}|^2} - \frac{1}{\pi} \text{Im}(\tilde{\sigma}) \right\} .$$

$\tilde{\pi}$ and $\tilde{\sigma}$ are taken directly from the graphical definition shown in Fig. 9,

$$\tilde{\pi}(z) = \iint d\varepsilon d\varepsilon' \tilde{\rho}^f(\varepsilon) \tilde{\rho}^f(\varepsilon') \frac{f(\varepsilon) - f(-\varepsilon')}{z - \varepsilon - \varepsilon'} , \quad (\text{C4a})$$

$$\tilde{\sigma}(z) = N_J V^2 \iint d\varepsilon d\varepsilon' \rho^c(\varepsilon) \tilde{\rho}^f(\varepsilon') \frac{f(\varepsilon) - f(-\varepsilon')}{z - \varepsilon - \varepsilon'} . \quad (\text{C4b})$$

The effect of a prefactor $[-1 - g(\omega)]$ to Eqs.(C4a) and (C4b) is made explicit by application of Eqs.(C2). Collecting the resulting parts together, we get

$$\begin{aligned} \tilde{\rho}^\Pi(\omega)[-1 - g(\omega)] = \left| \tilde{\Pi}(\omega) \right|^2 \\ \times \int d\varepsilon \left\{ \frac{\tilde{\rho}^f(\varepsilon)[1 - f(\varepsilon)]}{|\tilde{\pi}(\omega)|^2} + N_J V^2 \rho^c(\varepsilon) [1 - f(\varepsilon)] \right\} \\ \times \tilde{\rho}^f(\omega - \varepsilon) [1 - f(\omega - \varepsilon)] . \end{aligned}$$

Since $|\tilde{\pi}|^2 \gg \kappa$ the first term under the braces may be neglected with Eq.(4.7), and Eq.(4.21b) appears in writing \tilde{Z}/Z on both sides of the above formula. Furthermore, the result confirms the order of magnitude Eq.(4.16) directly for the special case of the ladder approximation.

APPENDIX D: SOME EXACT RELATIONS

1. Sum Rules

Exact sum rules are proven for spectra $\tilde{\rho}^f$, $\tilde{\rho}^\Pi$, $\overline{\rho}^f$, $\overline{\rho}^\Pi$, and the physical f -spectrum ρ^f . These are verified within the Self-Consistent T-Approximation. Results have already been stated in Section IV through Eqs.(4.22). The spin $\sigma = \pm 1$ is arbitrary in the following, since no external magnetic field is considered.

The total spectral weight of the propagator \tilde{G}^f is derived from Eq.(3.2a) as $\langle \{f_\sigma, f_\sigma^\dagger\} \rangle = 1$, accordingly the corresponding spectrum defined in Eq.(4.6) fulfills the sum rule Eq.(4.22a). In the same fashion, the spectral weight of $\tilde{\Pi}$ follows with Eqs.(4.17), (4.14) in the form

$$\begin{aligned} \int d\varepsilon \tilde{\rho}^\Pi(\varepsilon) = \tilde{\Pi}(0_-) - \tilde{\Pi}(0_+) \\ = \langle n_\uparrow^f n_\downarrow^f \rangle - \langle (1 - n_\uparrow^f)(1 - n_\downarrow^f) \rangle = \sum_\sigma \langle n_\sigma^f \rangle - 1 , \end{aligned}$$

and by introducing $\tilde{\rho}^f$ via $\langle n_\sigma^f \rangle = \int d\varepsilon \tilde{\rho}^f(\varepsilon) f(\varepsilon)$, the sum rule Eq.(4.22b) is confirmed.

In order to derive a sum rule for the Projected Spectra we first note the physical f -spectral-weight factor per spin,

$$\begin{aligned} \langle 1 - n_\sigma^f \rangle = -(\tilde{Z}/Z) \tilde{G}_\sigma^f(0_+) \\ = \frac{\tilde{Z}}{Z} \int d\varepsilon \tilde{\rho}^f(\varepsilon) [1 - f(\varepsilon)] = \int d\varepsilon \overline{\rho}^f(\varepsilon) . \end{aligned} \quad (\text{D1})$$

Consider also the probability of the local f -orbital being empty,

$$\begin{aligned} \langle (1 - n_\uparrow^f)(1 - n_\downarrow^f) \rangle = (\tilde{Z}/Z) \tilde{\Pi}(0_+) \\ = \frac{\tilde{Z}}{Z} \int d\varepsilon \tilde{\rho}^\Pi(\varepsilon) [-1 - g(\varepsilon)] = \int d\varepsilon \overline{\rho}^\Pi(\varepsilon) . \end{aligned} \quad (\text{D2})$$

In the last two expressions the respective first equality sign stems from the fact that states with doubly occupied f -orbital do not contribute to the traces (this has been explained in Section II B). At $U \rightarrow \infty$ the probability of double f -occupancy is zero, and with the probability $\langle n_\sigma^f(1 - n_{-\sigma}^f) \rangle$ for single f -occupancy a completeness relations holds,

$$\langle (1 - n_\uparrow^f)(1 - n_\downarrow^f) \rangle + \sum_\sigma \langle n_\sigma^f(1 - n_{-\sigma}^f) \rangle = 1 .$$

This leads with Eqs.(D1) and (D2) to the sum rule Eq.(4.22c) stated in Section IV .

The physical f -excitation spectrum is normalized according to Eq.(2.10), i.e.

$$\int d\varepsilon \rho^f(\varepsilon) = F_\sigma(0_-) - F_\sigma(0_+) = \langle 1 - n_{-\sigma}^f \rangle .$$

By use of Eq.(D1), the sum rule Eq.(4.22d) is evident.

A verification of sum rules in SCTA is performed for $\tilde{\rho}^f$ and $\tilde{\rho}^\Pi$ via the behavior of corresponding propagators at infinity,

$$|z| \rightarrow \infty : \tilde{G}^f(z) \rightarrow a^f/z, \tilde{\Pi}(z) \rightarrow a^\Pi/z .$$

From the self-consistency equations (4.18) at $|z| \rightarrow \infty$ we get

$$a^f = 1, a^\Pi = \int d\varepsilon \tilde{\rho}^f(\varepsilon)[2f(\varepsilon) - 1],$$

i.e. the values from exact sum rules Eqs.(4.22a) and (4.22b) are reproduced. The f -spectrum's normalization in SCTA is obtained via integration of Eq.(4.19),

$$\begin{aligned} \int d\omega \rho^f(\omega) &= \int d\omega \bar{\rho}^f(\omega) \int d\varepsilon \tilde{\rho}^\Pi(\varepsilon) + \int d\omega \bar{\rho}^\Pi(\omega) \\ &= 3 \int d\omega \bar{\rho}^f(\omega) - 1 . \end{aligned}$$

Corrections $\sim (\kappa)^1$ from application of the sum rule Eq.(4.22b) are negligible in the Kondo regime. Obviously the norm of ρ^f does not match the sum rule Eq.(4.22d).

2. Spectral Decomposition at Zero Temperature

Consider the unphysical spectra $\tilde{\rho}^f$ and $\tilde{\rho}^\Pi$ at zero temperature $T = 0$. A spectral decomposition of \tilde{G}_σ^f leads to $\tilde{\rho}_\sigma^f(\varepsilon) = \tilde{\rho}_\sigma^{f(+)}(\varepsilon) + \tilde{\rho}_\sigma^{f(-)}(\varepsilon)$ where

$$\tilde{\rho}_\sigma^{f(\pm)}(\varepsilon) = \sum_\alpha \left| \langle \Psi_\alpha | f_\sigma^{(\dagger)} | \Psi_0 \rangle \right|^2 \delta(\varepsilon \mp [E_\alpha - E_0])$$

at $T \rightarrow 0$. An f -creation operator f_σ^\dagger is used in $\tilde{\rho}_\sigma^{f(+)}$. The ground state $|\Psi_0\rangle$ of the Hamiltonian Eq.(2.11) in the full Fock space of f - and conduction electrons is $|\Psi_0\rangle = |2; \text{FS}^c\rangle$, a doubly occupied f -orbital plus the

filled Fermi sea of conduction electrons. It is unaffected by the perturbation in Eq.(2.11), and its energy $E_0 = 2\varepsilon^f + E^c$ is significantly lower than the ground state energy $E_G \approx E^c + \varepsilon^f - T_K$ of the ‘physical’ subspace $\mathcal{H}_{0,1}$ with f -occupancy ≤ 1 ; see also Sect. IV A. Since $f_\sigma^\dagger |2; \text{FS}^c\rangle \equiv 0$ and $f_\sigma |2; \text{FS}^c\rangle = \pm |-\sigma; \text{FS}^c\rangle$, it follows $\tilde{\rho}_\sigma^{f(+)}(\varepsilon) = 0$ and

$$\tilde{\rho}_\sigma^f(\varepsilon) = \sum_i |\langle \Psi_i | -\sigma; \text{FS}^c \rangle|^2 \delta(\varepsilon - [2\varepsilon^f + E^c - E_i]) .$$

From the complete set $\{|\Psi_\alpha\rangle\}$ of eigenstates only the subspace $\{|\Psi_i\rangle\} = \mathcal{H}_{0,1}$ contributes to the overlap integral, with energies $E_i \geq E_G$. Accordingly the spectrum $\tilde{\rho}_\sigma^f(\varepsilon) \sim \Theta(E^{Th} - \varepsilon)$ shows a threshold at energy $E^{Th} = 2\varepsilon^f - E_G + E^c$ slightly above the bare f -level ε^f . The same threshold emerges in $\tilde{\rho}^\Pi(\varepsilon) \sim \Theta(E^{Th} - \varepsilon)$: From a similar analysis $\tilde{\rho}^\Pi(\varepsilon)$ is obtained in the form of $\tilde{\rho}^f$ with $|-\sigma; \text{FS}^c\rangle$ replaced by $|0; \text{FS}^c\rangle$. At zero temperature the unphysical spectra $\tilde{\rho}_\sigma^f$ and $\tilde{\rho}^\Pi$ match the so-called ‘ionic spectra’ ρ_σ and ρ_0 of Resolvent-Perturbation Theory²³ via

$$\rho_\sigma(\varepsilon) = \tilde{\rho}_\sigma^f(2\varepsilon^f - \varepsilon), \rho_0(\varepsilon) = \tilde{\rho}^\Pi(2\varepsilon^f - \varepsilon) . \quad (\text{D3})$$

Accordingly an algebraic singularity is expected in $\tilde{\rho}^{f/\Pi}$ at energy approaching E^{Th} from below. It has nevertheless to be noted that the strict equality Eq.(D3) is lost at any finite temperature and is likely to be lost if approximations are considered (e.g. SCTA vs. NCA). Also is a relation like Eq.(D3) *not* found for the Projected Spectra introduced in Eq.(4.20) and the so-called Defect Spectra⁷⁶ (also called e.g. ‘negative-frequency spectra’⁷⁹) of NCA theory.

-
- ¹ G. Grüner and A. Zawadowski, in *Progress in Low Temperature Physics*, edited by D. F. Brewer (North-Holland, Amsterdam, 1978), Vol. 7B, Chap. 8, p. 593.
 - ² A. C. Hewson, *The Kondo Problem to Heavy Fermions* (Cambridge University Press, Cambridge, 1993).
 - ³ P. Fulde, J. Keller, and G. Zwicknagl, *Solid State Physics* **41**, 1 (1988).
 - ⁴ N. Grewe and F. Steglich, in *Handbook of the physics and chemistry of rare-earths*, edited by K. G. Gschneidner Jr. (North-Holland, Amsterdam, 1990), Vol. 14.
 - ⁵ P. Wyder (Ed.), *Physica C* **235-240**, (1994).
 - ⁶ P. W. Anderson, *Phys. Rev.* **124**, 41 (1961).
 - ⁷ J. Hubbard, *Proc. R. Soc. London Ser. A* **276**, 238 (1963).
 - ⁸ V. J. Emery, *Phys. Rev. Lett.* **58**, 2794 (1987).
 - ⁹ F. C. Zhang and T. M. Rice, *Phys. Rev. B* **37**, 3759 (1988).
 - ¹⁰ P. Nozières and A. Blandin, *J. Physique* **41**, 193 (1980).
 - ¹¹ D. C. Ralph and R. A. Buhrman, *Phys. Rev. Lett.* **69**, 2118 (1992).
 - ¹² D. C. Ralph, A. W. W. Ludwig, J. von Delft, and R. A. Buhrman, *Phys. Rev. Lett.* **72**, 1064 (1994).

- ¹³ M. H. Hetterl, J. Kroha, and S. Hershfield, Phys. Rev. Lett. **73**, 1967 (1994).
- ¹⁴ D. L. Cox, Phys. Rev. Lett. **59**, 1240 (1987).
- ¹⁵ M. B. Maple *et al.*, J. Low Temp. Phys. **95**, 225 (1994).
- ¹⁶ H. Keiter and J. C. Kimball, Int. J. Magn. **1**, 233 (1971).
- ¹⁷ C. Bloch and C. Dominicis, Nucl. Phys. **7**, 459 (1958).
- ¹⁸ H. Keiter and G. Morandi, Phys. Rep. **109**, 227 (1984).
- ¹⁹ N. E. Bickers, Rev. Mod. Phys. **59**, 846 (1987).
- ²⁰ N. Grewe and H. Keiter, Phys. Rev. B **24**, 4420 (1981).
- ²¹ Y. Kuramoto, in *Theory of Heavy Fermions and Valence Fluctuations*, edited by T. Kasuya and T. Saso (Springer, Berlin, 1985), p. 152.
- ²² N. Grewe, Z. Phys. B **67**, 323 (1987).
- ²³ For a review see e.g. Ref. 19.
- ²⁴ N. Read and D. M. Newns, J. Phys. C **16**, 3273 (1983).
- ²⁵ J. Rasul and H. U. Desgranges, J. Phys. C **19**, L671 (1986).
- ²⁶ A. Auerbach and K. Levin, Phys. Rev. Lett. **57**, 877 (1986).
- ²⁷ A. Millis and P. A. Lee, Phys. Rev. B **35**, 3394 (1987).
- ²⁸ P. Coleman, Phys. Rev. B **35**, 5072 (1987).
- ²⁹ H. Kaga and T. Yoshida, Physica C **159**, 727 (1989).
- ³⁰ M. U. Ubbens and P. A. Lee, Phys. Rev. B **49**, 6853 (1994).
- ³¹ D. M. Newns and N. Read, Adv. Physics **36**, 799 (1987).
- ³² P. Wölfle, J. Low Temp. Phys. **3&4**, 625 (1995).
- ³³ N. Read, J. Phys. C **18**, 2651 (1985).
- ³⁴ J. Brinckmann and N. Grewe, Z. Phys. B **84**, 179 (1991).
- ³⁵ J. C. L. Guillou and E. Ragoucy, Phys. Rev. B **52**, 2403 (1995).
- ³⁶ J. Hubbard, Proc. R. Soc. London Ser. A **296**, 82 (1966).
- ³⁷ W. Metzner, Phys. Rev. B **43**, 8549 (1991).
- ³⁸ M. Bartkowiak and K. A. Chao, Phys. Rev. B **47**, 4193 (1993).
- ³⁹ K. W. Becker and P. Fulde, Z. Phys. B **72**, 423 (1988).
- ⁴⁰ G. Polatsek, K. W. Becker, and V. Zevin, Phys. Rev. B **44**, 6062 (1991).
- ⁴¹ H. Keiter, Z. Phys. **214**, 22 (1968).
- ⁴² A. C. Hewson, J. Phys. C **10**, 4973 (1977).
- ⁴³ T. Yanagisawa, Phys. Rev. B **40**, 6666 (1989).
- ⁴⁴ Y. A. Izyumov and B. M. Letfulov, J. Phys.: Cond. Mat. **2**, 8905 (1990).
- ⁴⁵ M. L. Kulić, Sol. State Comm. **88**, 287 (1993).
- ⁴⁶ P. Coleman, Phys. Rev. B **29**, 3035 (1984).
- ⁴⁷ B. J. Yin and Y. Kuroda, J. Phys. Soc. Jpn. **57**, 1687 (1988).
- ⁴⁸ C. Gros and M. D. Johnson, Phys. Rev. B **40**, 9423 (1989).
- ⁴⁹ J. Brinckmann and N. Grewe, to be published.
- ⁵⁰ M. Gaudin, Nucl. Phys. **15**, 89 (1960).
- ⁵¹ J. Brinckmann, Europhys. Lett. **28**, 187 (1994).
- ⁵² J. Brinckmann, Physica B **206&207**, 171 (1995).
- ⁵³ J. R. Schrieffer and P. A. Wolff, Phys. Rev. **149**, 491 (1966).
- ⁵⁴ J. W. Negele and H. Orland, *Quantum Many-Particle Systems* (Addison-Wesley, Menlo Park etc., 1988).
- ⁵⁵ Strictly speaking, we have to use an unusual convergence factor $\exp(-i\omega_l 0_+)$ for a loop built from a single dashed line at a vertex in Fig. 1 (a), and a factor $\exp(i\omega_l 0_+)$ for a single dashed or full line closed onto itself at a vertex Fig. 1 (b) right. Other kinds of simple loops do not occur. In order to get the ‘global’ rule using only $\exp(-i\omega_l 0_+)$ as stated in the text, we have to turn operators in the second term of H^J , Eq.(2.4), to non-normal ordering ff^\dagger and cc^\dagger before applying Wick’s theorem. This results in a potential scattering for band electrons and a small shift of f -level ε^f which may be ignored.
- ⁵⁶ G. Toulouse, Phys. Rev. **2**, 270 (1970).
- ⁵⁷ J. Kondo, Prog. Theor. Phys. **32**, 37 (1964).
- ⁵⁸ A. A. Abrikosov, Physics **2**, 5 (1965).
- ⁵⁹ J. W. Rasul and A. C. Hewson, J. Phys. C **17**, 2555 (1984).
- ⁶⁰ U. Brandt, H. Keiter, and F. S. Liu, Z. Phys. B **58**, 267 (1985).
- ⁶¹ N. Grewe, Z. Phys. B **52**, 193 (1983).
- ⁶² Y. Kuramoto, Z. Phys. B **53**, 37 (1983).
- ⁶³ T. K. Lee and F. C. Zhang, Phys. Rev. B **30**, 1556 (1984).
- ⁶⁴ H. R. Krishna-murthy, J. W. Wilkins, and K. G. Wilson, Phys. Rev. B **21**, 1044 (1980).
- ⁶⁵ A. M. Tselik and P. B. Wiegmann, Adv. in Phys. **32**, 453 (1983).
- ⁶⁶ P. Schlottmann, Phys. Rep. **181**, 1 (1989).
- ⁶⁷ J. M. Luttinger and J. C. Ward, Phys. Rev. **118**, 1417 (1960).
- ⁶⁸ The discussion in Note 55 remains valid for skeleton diagrams, since the only closed fermion loop to be considered in addition is that built of a single mix-Green’s function $\tilde{G}_\sigma^{fc/cf}$: It’s spectral function is normalized to Null, therefore a convergence factor has no effect and is arbitrary.
- ⁶⁹ P. Nozières, J. Gavoret, and B. Roulet, Phys. Rev. **178**, 1084 (1969).
- ⁷⁰ N. E. Bickers, in *Strongly Correlated Electron Systems II*, Vol. 29 of *Proc. Adriatico Res. Conf.*, edited by G. Baskaran, A. E. Ruckenstein, E. Tosatti, and Y. Lu (World Scientific, Singapore, 1991), p. 253.
- ⁷¹ Compare e.g. to Ref. 54.
- ⁷² For the analytical solution of mean-field equations at $T \rightarrow 0$ and $V \ll |\varepsilon^f| < D$, $\varepsilon^f < 0$ one may rely on slave-boson treatments (see e.g. Ref. 31). Our mean-field equations can be reproduced formally from the slave-boson equations³¹, if the degeneracy N_J in the latter is set to $N_J = 1$. Thus a trivial solution is to be expected in the present case.
- ⁷³ J. Brinckmann, Doctoral Dissertation, Technische Hochschule Darmstadt 1995 (unpublished).
- ⁷⁴ G. Baym, Phys. Rev. **127**, 1391 (1962).
- ⁷⁵ This is a consequence of $1 + g(\omega) \sim \text{sgn}(\omega)$ and $\tilde{\rho}^\Pi(\omega) \sim -\text{sgn}(\omega)$. The latter follows from the fact that $\tilde{\Pi}$ defined in Eq.(4.17) is a bosonic double-time Green’s function of the form $\langle \mathcal{T}\{A(\tau)A^\dagger(\tau')\} \rangle$.
- ⁷⁶ E. Müller-Hartmann, Z. Phys. B **57**, 281 (1984).
- ⁷⁷ K. Yosida and K. Yamada, Prog. Theor. Phys. **53**, 1286 (1975).
- ⁷⁸ A. Yoshimori and A. Zawadowski, J. Phys. C. **15**, 524 (1982).
- ⁷⁹ N. E. Bickers, D. L. Cox, and J. W. Wilkins, Phys. Rev. B **36**, 2036 (1987).
- ⁸⁰ R. Brout, Phys. Rev. **122**, 469 (1961).
- ⁸¹ N. Grewe, Sol. State Comm. **50**, 19 (1984).
- ⁸² N. Grewe, T. Pruschke, and H. Keiter, Z. Phys. B **71**, 75

- (1988).
- ⁸³ C. I. Kim, Y. Kuramoto, and T. Kasuya, J. Phys. Soc. Jpn. **59**, 2414 (1990).
- ⁸⁴ W. Metzner and D. Vollhardt, Phys. Rev. Lett. **62**, 324 (1989).
- ⁸⁵ E. Müller-Hartmann, Z. Phys. B **74**, 507 (1989).
- ⁸⁶ Y. Kuramoto and T. Watanabe, Physica **148 B**, 80 (1987).
- ⁸⁷ H. Schweitzer and G. Czycholl, Z. Phys. B **74**, 303 (1989).
- ⁸⁸ U. Brandt and C. Mielsch, Z. Phys. B **79**, 295 (1990).
- ⁸⁹ P. G. J. van Dongen and D. Vollhardt, Phys. Rev. Lett. **65**, 1663 (1990).
- ⁹⁰ V. Janiš, Z. Phys. B **83**, 227 (1991).
- ⁹¹ M. Jarrell, Phys. Rev. Lett. **69**, 168 (1992).
- ⁹² A. Georges, G. Kotliar, and Q. Si, Int. J. Mod. Phys. B **6**, 705 (1992).
- ⁹³ G. Hülshenbeck and Q. Qin, Sol. State Comm. **90**, 195 (1994).
- ⁹⁴ H. Keiter, T. Leuders, C. Melsheimer, and P. Schönenberg, Physica B **206&207**, 168 (1995).
- ⁹⁵ C. I. Kim, Y. Kuramoto, and T. Kasuya, Sol. State Comm. **62**, 627 (1987).
- ⁹⁶ F. Anders, J. Phys.: Cond. Mat. **7**, 2801 (1995).
- ⁹⁷ T. A. Costi, J. Kroha, and P. Wölfle, Phys. Rev. B **53**, 1850 (1996).
- ⁹⁸ K. Ingersent, B. A. Jones, and J. W. Wilkins, Phys. Rev. Lett. **69**, 2594 (1992).
- ⁹⁹ B. Batlogg *et al.*, Physica C **235-240**, 130 (1994).
- ¹⁰⁰ Z.-X. Shen and D. S. Dessau, Physics Rep. **253**, 1 (1995).
- ¹⁰¹ F. Steglich *et al.*, J. Low Temp. Phys. **95**, 3 (1994).
- ¹⁰² M. Jarrell, H. Akhlaghpour, and T. Pruschke, Phys. Rev. Lett. **70**, 1670 (1993).
- ¹⁰³ M. Jarrell, Phys. Rev. B **51**, 7429 (1995).
- ¹⁰⁴ M. J. Rozenberg, Phys. Rev. B **52**, 7369 (1995).
- ¹⁰⁵ T. Mutou and D. S. Hirashima, J. Phys. Soc. Jpn. **63**, 4475 (1994).
- ¹⁰⁶ H. Schweitzer and G. Czycholl, Z. Phys. B **79**, 377 (1990).
- ¹⁰⁷ K. A. Chao, J. Spalek, and A. M. Oleś, J. Phys. C **10**, L271 (1977).

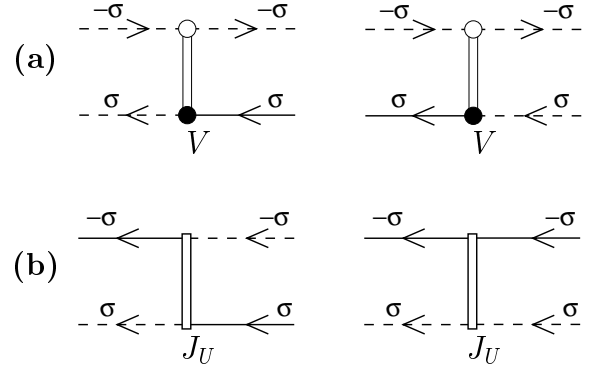


FIG. 1. Vertices of the Feynman-diagram expansion. Dashed lines correspond to local Green's functions $\tilde{G}^{f(0)}$, Eq.(2.16), full lines stand for conduction-electron propagators G^c , Eq.(2.17). Vertices (a) originate from H_{01}^V (see Eq.(2.1c)) and are interpreted in the subspace without doubly occupied local f -orbital: A transfer band- to f -electron (left) or vice versa (right) is permitted only if a f -hole of opposite spin is present. In (b) the spin-flip and charge scattering vertex of H^J (see Eq.(2.4)) are shown on the left and right, respectively.

$$\gamma_{\sigma}^{pp}(i\nu_k) = i\nu_k \begin{array}{c} \bullet \leftarrow \sigma \\ \leftarrow \sigma \\ \bullet \leftarrow \sigma \\ \leftarrow \sigma \end{array} i\nu_k$$

$$\gamma_{\sigma}^{ph}(i\nu_k) = i\nu_k \begin{array}{c} \bullet \leftarrow \sigma \\ \leftarrow \sigma \\ \bullet \leftarrow \sigma \\ \leftarrow \sigma \end{array} i\nu_k$$

$$\gamma_{\sigma}^{p\bar{h}}(i\nu_k) = i\nu_k \begin{array}{c} \bullet \leftarrow \sigma \\ \leftarrow \sigma \\ \bullet \leftarrow \sigma \\ \leftarrow \sigma \end{array} i\nu_k$$

FIG. 2. Simple ladder diagrams from particle-particle (pp) and particle-hole ($ph, p\bar{h}$) vertex contributions to the f -Green's function at $U \rightarrow \infty$. These may show logarithmic divergences, see text.

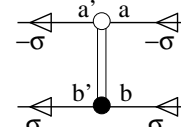
(a) $\bar{G}_\sigma^f(i\omega_l) = \begin{array}{c} i\omega_l \\ \vdots \\ \sigma \end{array} \leftarrow \leftarrow \leftarrow \leftarrow \leftarrow$ $\bar{G}_\sigma^{fc}(i\omega_l) = \begin{array}{c} i\omega_l \\ \vdots \\ \sigma \end{array} \leftarrow \leftarrow \leftarrow \leftarrow \leftarrow \leftarrow$

(b) $\bar{G}_\sigma^{cf}(i\omega_l) = \begin{array}{c} i\omega_l \\ \leftarrow \leftarrow \leftarrow \leftarrow \leftarrow \\ \sigma \end{array}$ $\bar{G}_\sigma^c(i\omega_l) = \begin{array}{c} i\omega_l \\ \leftarrow \leftarrow \leftarrow \leftarrow \leftarrow \\ \sigma \end{array}$

(c) $\mathbf{G}_\sigma(i\omega_l) = \begin{array}{c} i\omega_l \\ \leftarrow \leftarrow \leftarrow \leftarrow \leftarrow \\ \sigma \end{array}$ $\mathbf{G}_\sigma^{(0)}(i\omega_l) = \begin{array}{c} i\omega_l \\ \leftarrow \leftarrow \leftarrow \leftarrow \\ \sigma \end{array}$

(c) $\begin{array}{c} i\omega_l \\ \leftarrow \leftarrow \leftarrow \leftarrow \leftarrow \\ \sigma \end{array} = \begin{array}{c} i\omega_l \\ \leftarrow \leftarrow \leftarrow \leftarrow \leftarrow \\ \sigma \end{array} + \begin{array}{c} i\omega_l \\ \leftarrow \leftarrow \leftarrow \leftarrow \leftarrow \\ \sigma \end{array} \circlearrowleft \begin{array}{c} i\omega_l \\ \leftarrow \leftarrow \leftarrow \leftarrow \leftarrow \\ \sigma \end{array}$

FIG. 3. (a): Notation of renormalized Green's functions occurring in skeleton diagrams of the $U \rightarrow \infty$ problem. A definition is given in Eq.(3.2). (b): 2×2 -matrix-Green's function (left), its matrix elements are shown in (a), and corresponding bare propagator (right). (c): Dyson's equation involving matrix-self energy Eq.(3.4).

(a)  $= V \begin{pmatrix} 1 & 0 \\ 0 & 0 \end{pmatrix}^{a'a} \begin{pmatrix} 0 & 1 \\ 1 & 0 \end{pmatrix}^{b'b}$

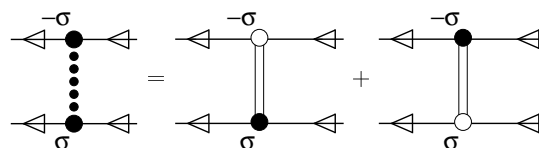
(b) 

FIG. 4. (a): Vertex used with matrix-Green's function from Fig. 3 (b) for $U \rightarrow \infty$. It collects both hybridization types shown in Fig. 1 (a). 'Spinor' indices $a^{(l)}, b^{(l)} = 1^{(l)}, 2^{(l)}$ indicate canonical operators $1^{(l)} \equiv f^{(t)}$, $2^{(l)} \equiv C^{(t)}$. (b): Vertex combination used in expansion of matrix-self energy Σ .

$\Sigma_\sigma(i\omega_l) = \begin{array}{c} i\omega_l \\ \leftarrow \leftarrow \leftarrow \leftarrow \leftarrow \\ \sigma \end{array} \circlearrowleft \begin{array}{c} i\omega_l \\ \leftarrow \leftarrow \leftarrow \leftarrow \leftarrow \\ \sigma \end{array} + \begin{array}{c} i\omega_l \\ \leftarrow \leftarrow \leftarrow \leftarrow \leftarrow \\ \sigma \end{array} \circlearrowleft \begin{array}{c} i\omega_l \\ \leftarrow \leftarrow \leftarrow \leftarrow \leftarrow \\ \sigma \end{array} \text{---} \Gamma_P^2 \text{---} \begin{array}{c} i\omega_l \\ \leftarrow \leftarrow \leftarrow \leftarrow \leftarrow \\ \sigma \end{array}$

FIG. 5. Exact skeleton representation of matrix-self energy at $U \rightarrow \infty$, with full Green's function and vertex from Figs. 3 (b) and 4 (b). Due to the vertex' spin restriction no 'Fock diagram' is present. All higher orders are collectively expressed through the irreducible vertex function Γ_P^2 .

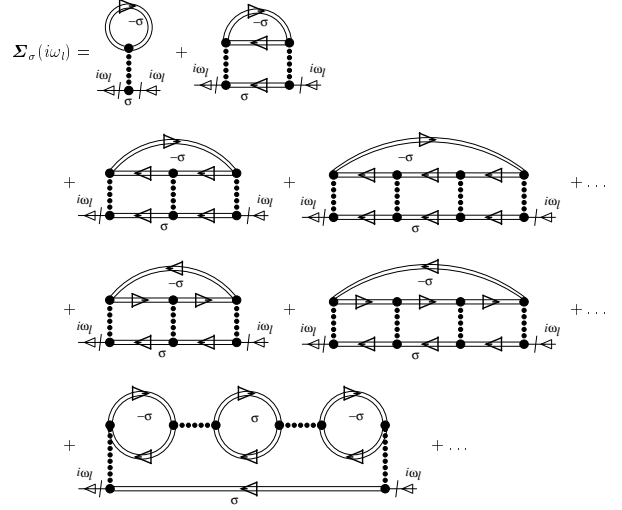


FIG. 6. Self energy in Self-Consistent T-Approximation. With spin restriction at vertices, all exchange parts present in the vertex function in Fig. 5 do not contribute to Σ and internal spin sums do not occur. The self energy is exact to V^2 (first row), higher orders separate into ladder sums from (pp)-channel (2nd row) and (ph)- (3rd row) and (\overline{ph})-channels (4th row).

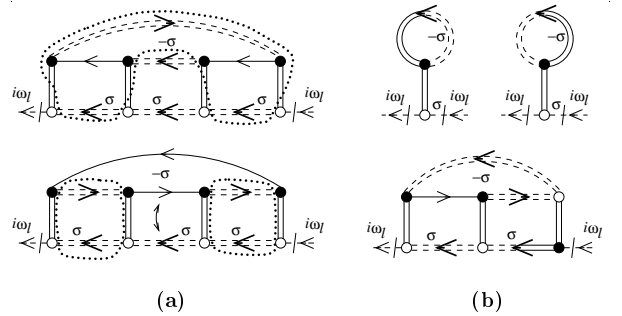


FIG. 7. Examples of diagrams to Σ^{ff} which do not contribute in the Kondo regime: (a): due to the *loop theorem* (possible closed paths are indicated by dotted lines); (b): due to the presence of \tilde{G}^{fc} or \tilde{G}^{cf} . Notation follows Fig. 3 (a).

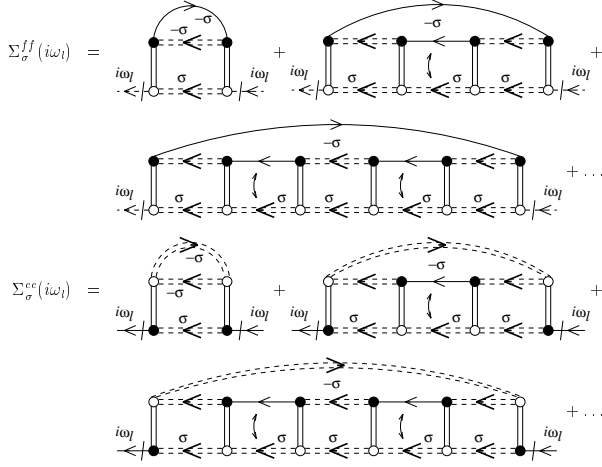


FIG. 8. Self energy Σ in the Kondo regime, consisting only of (pp) -type diagrams with Green's functions \tilde{G}^f (dashed double line) and bare conduction electrons G^c (full lines). Off-diagonal elements Σ^{cf} and Σ^{fc} as well as all (ph) - and $(\bar{p}\bar{h})$ -type diagrams included in Fig. 6 are negligible in the Kondo regime, examples are shown in Fig. 7. In each plaquette indicated by a small double arrow, parallel band- and f -lines may be interchanged, leading to the full set of diagrams to be considered.

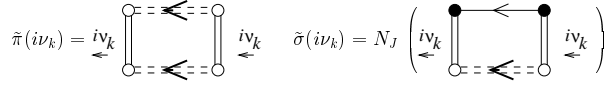


FIG. 9. Definition of 'ladder elements' occurring in Fig. 8. Spin degeneracy leads to the prefactor $N_J \equiv 2$ in $\tilde{\sigma}(i\nu_k)$.

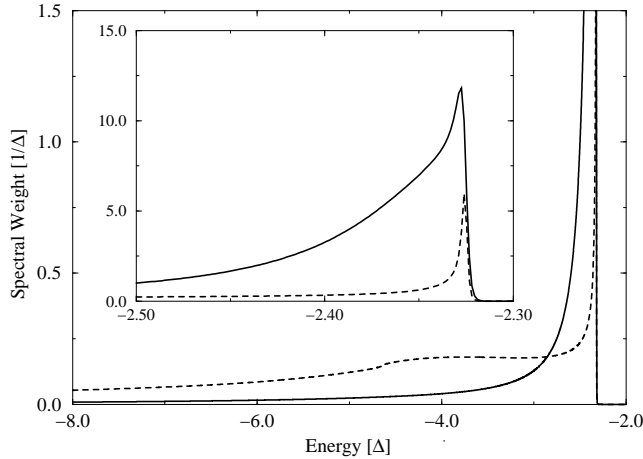


FIG. 10. Spectra $\tilde{\rho}^f$ (full line) and $\tilde{\rho}^\Pi$ (dashed line) from numerical solution of SCTA equations (see text). Parameters are $\varepsilon^f = -3.0\Delta$, $D = 10.0\Delta$, $N_J \equiv 2$, and $k_B T = 0.1T_K$. The spectral weight turns to zero for energies above the threshold. **Inset:** Neighborhood of the threshold (note the different vertical scale).

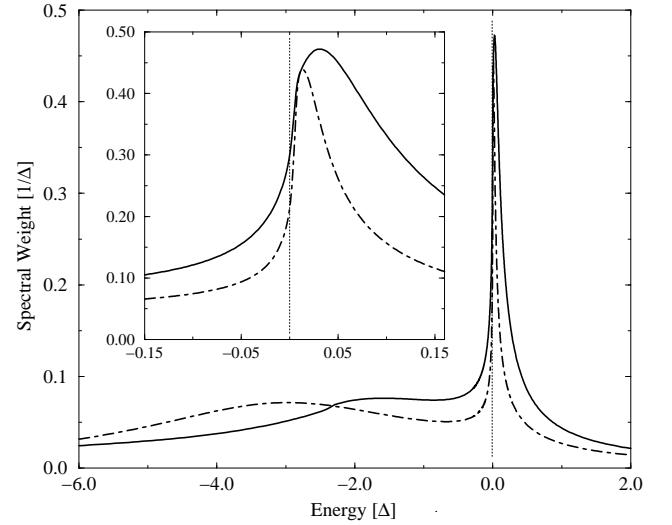


FIG. 11. Local f -excitation spectrum of the $U \rightarrow \infty$ Anderson model from Self-Consistent T-Approximation (full line) and NCA (dashed dotted line). **Inset:** Abrikosov-Suhl resonance near the Fermi energy $\omega = 0$. Parameters as in Fig. 10.